



**Hydraulics Research**  
Wallingford

THE DEVELOPMENT OF A NUMERICAL MODEL  
FOR THE SOLUTION OF THE BOUSSINESQ  
EQUATIONS FOR SHALLOW WATER WAVES

Variable depth case

D V Jones BSc, PhD  
J V Smallman BSc, PhD

Report No SR 159  
February 1988

Registered Office: Hydraulics Research Limited,  
Wallingford, Oxfordshire OX10 8BA.  
Telephone: 0491 35381. Telex: 848552

© Crown Copyright 1988. Published by permission of the Controller of Her Majesty's Stationery Office.

This report describes work supported under contract PECD 7/6/053 funded by the Department of the Environment. The DOE nominated officer was Dr R Thorogood. Dr S W Huntington was Hydraulics Research's nominated officer. The report is published with the permission of the Department of the Environment but any opinions expressed are not necessarily those of the funding department.

The development of a numerical model for the solution of the Boussinesq equations for shallow water waves. Variable depth case. D V Jones and J V Smallman, Report No SR 159, February 1988.

#### ABSTRACT

This report describes the further development of a finite difference model which was originally formulated to solve the Boussinesq equations in water of constant depth. The main objective of the work reported here was to extend the mathematical model to allow the effects of depth variation to be included. In addition, changes were also made to the existing model boundary conditions to allow a random wave train to be specified as input.

The first stage in the implementation of the varying depth terms was to extend the predictor-corrector finite difference scheme so that advantage could be taken of the computer power of the distributed array processor (DAP). Once this was complete the model was tested first for a one-dimensional sloping bed to check that shoaling was correctly represented. The results from the model for this case were compared with theoretical solutions, and the agreement was found to be good.

A series of tests were then carried out to test the two dimensional case. These involved both tests to examine linear and non-linear refraction and shoaling, and also diffraction by breakwaters in varying depth. Good agreement was found between the model results, theoretical solutions and the results from other mathematical models where these were available.

The remainder of the report describes the implementation of random wave boundary conditions in the model. Comparisons were made with theoretical results and it was found that the numerical model gave a reasonable representation of set down effects for a random wave train in water of constant depth. It was recommended that further tests should be carried out to examine these effects in water of varying depth, once physical model results are available for comparison. This would allow the numerical model with random wave input to be tested more rigorously.

In conclusion, the extended numerical model was found to give a good representation of the effects of refraction and shoaling, and diffraction by breakwaters in varying depth. The model also successfully reproduced the effects of set down beneath a random wave train in water of constant depth.



## CONTENTS

	Page
1 INTRODUCTION	1
2 SOLUTION FOR VARYING DEPTH	1
2.1 Outline of approach	1
2.2 The finite difference scheme	4
2.3 Numerical results	6
2.3.1 Solution of linear shallow water equations	7
2.3.2 The effect of introducing dispersion	11
2.3.3 The extension to two dimensions by including refraction	13
2.3.4 The introduction of non-linear terms	17
2.3.5 Diffraction from the corner of a wedge breakwater	20
2.3.6 Diffraction of a breakwater gap, with constant water depth	21
2.4 Summary	22
3 RANDOM INCIDENT WAVES	23
3.1 Background	23
3.2 Boundary conditions	24
3.3 Implementation and verification	27
4 CONCLUSIONS AND RECOMMENDATIONS	33
4.1 Conclusions	33
4.2 Recommendations	33
5 ACKNOWLEDGEMENTS	34
6 REFERENCES	35

## TABLES

1. Results with bathymetry A: numerical solution of equations (2.4) and (2.5)
2. Results with bathymetry A: numerical solution of equations (2.6) and (2.7)
3. Results with bathymetry A: numerical solution of equations (2.8) and (2.10)
4. Results with bathymetry C: numerical solution of equations (2.8) and (2.10)
5. The non-linear problem with bathymetry A: numerical solution of one dimensional form of equations (2.1) - (2.3)
6. The non-linear problem with bathymetry B: numerical solution of equations (2.1) - (2.3)
7. Results with bathymetry D: numerical solution of the linear (equations (2.8) - (2.10)) and non-linear (equations (2.1) - (2.3)) problems

## CONTENTS (CONT/D)

### TABLES (CONT/D)

8. Results for the breakwater gap problem, and comparison with theoretical results
9. Random wave tests for regular wave groups with primary frequencies 0.07Hz. Water depth 10m,  $\Delta x = 5m$ ,  $\Delta t = 0.34s$ . Expected wave amplitudes are 0.75m at  $f = 0.03Hz$  0.3m at  $f = 0.07Hz$  and 0.5m at  $f = 0.10Hz$
10. Random wave tests with Pierson Moskowitz spectrum  $T_p = 10s$  Water depth = 10m,  $\Delta x = 5m$ ,  $\Delta t = 0.34s$ , 1024 time steps analysed,  $\Delta f = 0.0115Hz$

### FIGURES

1. Profile and plan of bathymetry A : One dimensional shoal
2. Profile and plan of bathymetry B : Shoal and refraction
3. Profile and plan of bathymetry C : Alternative shoal and refraction
4. Profile and plan of bathymetry D : Alternative shoal and refraction with wedge breakwater
5. Numerical solution of 1D linear shallow water equations, see eqns (2.4) & (2.5), for bathymetry A, period  $T = 6s$ . Input wave amplitude = 1.0m
6. Numerical solution of 1D linear shallow water equations, see eqns (2.4) & (2.5), for bathymetry A, period  $T = 10s$ . Input wave amplitude = 1.0m
7. Numerical solution of 1D linear shallow water equations, see eqns (2.4) & (2.5), for bathymetry A, period  $T = 15s$ . Input wave amplitude = 1.0m
8. Wave elevation plotted against time at four surface points, period  $T = 10s$ , with bathymetry A. Numerical solution of equations (2.4) & (2.5). Input wave amplitude = 1.0m
9. Numerical results showing the effect of introducing dispersion. Solution of equations (2.6) & (2.7), bathymetry A,  $T = 6s$ . Input wave amplitude = 1.0m
10. Numerical results showing the effect of introducing dispersion. Solution of equations (2.6) & (2.7), bathymetry A,  $T = 10s$ . Input wave amplitude = 1.0m
11. Numerical results showing the effect of introducing dispersion. Solution of equations (2.6) & (2.7), bathymetry A,  $T = 15s$ . Input wave amplitude = 1.0m
12. Wave elevation plotted against time at three surface points, period  $T = 15s$ , with bathymetry A. Numerical solution of equations (2.6) and (2.7). Input wave amplitude = 1.0m
13. Numerical solution of 2 dimensional linear water equations (eqns (2.8) - (2.10)) for bathymetry B, period  $T = 6s$ . Input wave amplitude = 1.0m
14. Numerical solution of 2 dimensional linear water equations (eqns (2.8) - (2.10)) for bathymetry B, period  $T = 10s$ . Input wave amplitude = 1.0m
15. Numerical solution of 2 dimensional linear water equations (eqns (2.8) - (2.10)) for bathymetry B, period  $T = 15s$ . Input wave amplitude = 1.0m

## CONTENTS (CONT/D)

### FIGURES (CONT/D)

16. Wave elevation plotted against time at three surface points, period  $T = 10s$ , bathymetry B. Numerical solution of equations (2.8) - (2.10). Input wave amplitude = 1.0m
17. Numerical solution of linearised water equations (eqn (2.8) - (2.10)), with bathymetry C, period  $T = 6s$ , and comparison with results of a different numerical model. Input wave amplitude = 0.5m
18. Numerical solution of linearised water equations (eqns (2.8) - (2.10)) with bathymetry C, period  $T = 10s$ , and comparison with results of a different numerical model. Input wave amplitude = 0.5m
19. Surface wave elevation across part of basin with bathymetry C, for period  $T = 15s$ , at times 50s, 100s, 150s and 200s after start. ( $\Delta T = 0.25s$ )
20. Numerical solution of non-linear water equations (see eqns (2.1) - (2.3)), with bathymetry A, period  $T = 6s$ . Input wave amplitude = 0.35m
21. Numerical solution of non-linear water equations (see eqns (2.1) - (2.3)), with bathymetry A, period  $T = 10s$ . Input wave amplitude = 0.1m
22. Numerical solution of non-linear water equations (see eqns (2.1) - (2.3)), with bathymetry B, period  $T = 10s$ . Input wave amplitude = 0.1m
23. Wave elevation plotted against time at point 11 and 12, bathymetry A (see Fig 1), non-linear solution, period  $T = 6s$ . Input wave amplitude = 0.35m
24. Wave elevation plotted against time at points 11 and 12, bathymetry A (see Fig 1), non-linear solution, period  $T = 10s$ . Input wave amplitude = 0.1m
25. Surface wave elevation for non-linear waves, period  $T = 10s$ , 70.32s after start, for (a) bathymetry A, (b) bathymetry B ( $\Delta t = 0.3516s$ )
26. Linear and non-linear numerical solutions with a wedge (bathymetry D), period  $T = 10s$ . Input wave amplitude = 0.1m
27. Wave elevation plotted against time at point 12, bathymetry D, period  $T = 10s$ , comparing the linear and non-linear solutions. Input wave amplitude = 0.1m
28. Surface wave elevation part of basin with bathymetry D, for non-linear waves. Period  $T = 10s$ , elevation shown at times 46.88s, 93.76s, 140.64s and 187.52s after start. ( $\Delta t = 0.2344s$ )
29. Breakwater gap configuration, for 10s period incident wave. Gap width = 1.75 x (wavelength)
30. Diffraction by a breakwater gap, with constant water depth
31. Wave elevation plotted against time at two surface points, period  $T = 10s$ , for breakwater gap (see Fig 29) input amplitude = 1.0m
32. Surface elevations - regular wave groups
33. Spectrum for random wave input
34. Spectral densities for Pierson-Moskowitz input
35. Surface elevations - random wave groups

### APPENDIX

1. Derivation of set down amplitudes



## 1 INTRODUCTION

The development of a numerical model for the solution of the Boussinesq equations for shallow water waves in water of constant depth was described in a report by Smallman et al (Ref 1). Two specific recommendations given there were that in order to represent more realistic situations the numerical model should be developed further to include the effects of varying depth, and to allow random incident waves. The present report gives details of the implementation both of these aspects into the existing numerical model.

The remainder of this report is divided into three main chapters. A discussion of the Boussinesq equations for varying depth is given in Chapter 2, together with a description of the numerical method which was used to solve them. Several test problems were solved using these equations for various bathymetries. The results from these tests are also given in Chapter 2, together with details of comparisons with theoretical solutions and other numerical models. The implementation of a random wave input into the Boussinesq model is described in Chapter 3. Details are also given in this chapter of tests which were carried out to ensure that the model was operating correctly with random incident waves. The conclusions and recommendations arising from the research described in this report are given in the final chapter.

## 2 SOLUTION FOR VARYING DEPTH

### 2.1 Outline of approach

The two dimensional Boussinesq wave equations were given in a previous report (Smallman et al, (Ref 1),

where their derivation and meaning were explained.

For convenience they are restated here:

$$\frac{\partial z}{\partial t} + \frac{\partial}{\partial x} (uh) + \frac{\partial}{\partial y} (vh) = 0 \quad (2.1)$$

$$\begin{aligned} \frac{\partial u}{\partial t} + u \frac{\partial u}{\partial x} + v \frac{\partial u}{\partial y} = & -g \frac{\partial z}{\partial x} + \frac{1}{2} d \left[ \frac{\partial^3 (ud)}{\partial x^2 \partial t} + \frac{\partial^3 (vd)}{\partial x \partial y \partial t} \right] \\ & - \frac{1}{6} d^2 \left[ \frac{\partial^3 u}{\partial x^2 \partial t} + \frac{\partial^3 v}{\partial x \partial y \partial t} \right] \end{aligned} \quad (2.2)$$

$$\begin{aligned} \frac{\partial v}{\partial t} + u \frac{\partial v}{\partial x} + v \frac{\partial v}{\partial y} = & -g \frac{\partial z}{\partial y} + \frac{1}{2} d \left( \frac{\partial^3 (ud)}{\partial x \partial y \partial t} + \frac{\partial^3 (vd)}{\partial y^2 \partial t} \right) \\ & - \frac{1}{6} d^2 \left( \frac{\partial^3 u}{\partial x \partial y \partial t} + \frac{\partial^3 v}{\partial y^2 \partial t} \right) \end{aligned} \quad (2.3)$$

where  $u$  and  $v$  are depth averaged velocity components ( $\text{ms}^{-1}$ ) in the horizontal  $x$  and  $y$  directions respectively,  $z$  is the water surface elevation (m) above datum, which is the still water level, and  $h = d+z$ , where  $d$  is the mean water depth (m). In Ref 1, the equations were solved for the case where the depth  $d$  was everywhere constant. We now consider the more general case where the depth varies as a function of  $x$  and  $y$ .

In order to include the effect of depth variation, we need to solve equations (2.1) to (2.3) which involve terms including the differentials of  $(ud)$  or  $(vd)$ . To do this it is necessary to modify the finite difference scheme which was used to solve the equations for the constant depth case. This modification to the finite difference scheme is explained in Section 2.2.

To gain understanding of the behaviour of the numerical model with varying depth, the problem has been considered in four stages. The simplest of these is given by the one dimensional linear shallow water equations, which are obtained by neglecting the third

order and non-linear terms in the one dimensional form of equations (2.1) to (2.3):

$$\frac{\partial z}{\partial t} + \frac{\partial}{\partial x} (uh) = 0 \quad (2.4)$$

$$\frac{\partial u}{\partial t} + g \frac{\partial z}{\partial x} = 0 \quad (2.5)$$

The numerical model has been used to solve these equations for a one-dimensional shoal, that is the case in which the waves are normally incident on a sloping bed with parallel contours (see Fig 1). The results from the numerical model for this case are described in Section 2.3.1.

The next stage was to extend equations (2.4) and (2.5) by including the dispersive, third order terms:

$$\frac{\partial z}{\partial t} + \frac{\partial}{\partial x} (uh) = 0 \quad (2.6)$$

$$\frac{\partial u}{\partial t} + g \frac{\partial z}{\partial x} = \frac{1}{2} d \left( \frac{\partial^3 (ud)}{\partial x^2 \partial t} \right) - \frac{1}{6} d^2 \left( \frac{\partial^3 u}{\partial x^2 \partial t} \right) \quad (2.7)$$

These equations were solved numerically for the same bathymetry as was used for equations (2.4) and (2.5). The model results are described in detail in Section 2.3.2.

The next stage was to consider an extension to two dimensions of equations (2.6) and (2.7). This is equivalent to linearising equations (2.1) to (2.3), which results in the following:

$$\frac{\partial z}{\partial t} + \frac{\partial}{\partial x} (uh) + \frac{\partial}{\partial y} (vh) = 0 \quad (2.8)$$

$$\frac{\partial u}{\partial t} = -g \frac{\partial z}{\partial x} + \frac{1}{2} d \left[ \frac{\partial^3 (ud)}{\partial x^2 \partial t} + \frac{\partial^3 (vd)}{\partial x \partial y \partial t} \right] \quad (2.9)$$

$$- \frac{1}{6} d^2 \left[ \frac{\partial^3 u}{\partial x^2 \partial t} + \frac{\partial^3 v}{\partial x \partial y \partial t} \right]$$

$$\frac{\partial v}{\partial t} = -g \frac{\partial z}{\partial y} + \frac{1}{2} d \left( \frac{\partial^3 (ud)}{\partial x \partial y \partial t} + \frac{\partial^3 (vd)}{\partial y^2 \partial t} \right) \quad (2.10)$$

$$- \frac{1}{6} d^2 \left( \frac{\partial^3 u}{\partial x \partial y \partial t} + \frac{\partial^3 v}{\partial y^2 \partial t} \right)$$

The solution to these equations was found for bathymetries which allow both shoaling and refraction of the waves to take place (see Figs 2 and 3). In addition, a breakwater was introduced to study diffraction (see Fig 4). These results are discussed in Sections 2.3.3 and 2.3.5.

Finally, the full non-linear problem given by equations (2.1) to (2.3) was solved. This was done firstly for a one dimensional shoal, secondly for the bathymetry which allows shoaling and refraction, and lastly for a case where diffraction by a breakwater was represented. The solutions of the two dimensional non-linear problem are discussed in Sections 2.3.4 and 2.3.5.

## 2.2 The finite difference scheme

The finite difference scheme described in Ref 1 was formulated to solve the constant depth form of equations (2.1) to (2.3). Some modifications to the scheme given in Reference 1 are required to the third order terms, to allow for a varying depth. The finite difference approximations to the differentials of  $u$  and  $v$ , which form the last terms of equations (2.2) and (2.3) here, can be derived from the constant depth scheme simply by changing their coefficients from  $1/3$  to  $-1/6$ . The differentials of  $ud$  and  $vd$ , which form

the penultimate terms in equations (2.2) and (2.3), require additions to the scheme.

The differential operators are identical to those for constant depth, and so the finite difference description of the terms can be written immediately. In the notation of Ref 1,

$$\begin{aligned} \left[ \frac{\partial^3 (ud)}{\partial x^2 \partial t} \right]_{i, j-\frac{1}{2}}^n &= \\ \frac{1}{2\Delta t (\Delta x)^2} & \left[ (ud)_{i+1, j-\frac{1}{2}}^{n+\frac{1}{2}} - 2(ud)_{i, j-\frac{1}{2}}^{n+\frac{1}{2}} + (ud)_{i-1, j-\frac{1}{2}}^{n+\frac{1}{2}} \right. \\ & \left. - (vd)_{i+1, j-\frac{1}{2}}^{n-\frac{1}{2}} + 2(ud)_{i, j-\frac{1}{2}}^{n-\frac{1}{2}} - (ud)_{i-1, j-\frac{1}{2}}^{n-\frac{1}{2}} \right] \end{aligned} \quad (2.11)$$

$$\begin{aligned} \left[ \frac{\partial^3 (vd)}{\partial x \partial y \partial t} \right]_{i, j-\frac{1}{2}}^n &= \\ \frac{1}{2\Delta x \Delta y \Delta t} & \left[ (vd)_{i+\frac{1}{2}, j}^{n+\frac{1}{2}} - (vd)_{i-\frac{1}{2}, j}^{n+\frac{1}{2}} - (vd)_{i+\frac{1}{2}, j-1}^{n+\frac{1}{2}} + (vd)_{i-\frac{1}{2}, j-1}^{n+\frac{1}{2}} \right. \\ & \left. - (vd)_{i+\frac{1}{2}, j}^{n-\frac{1}{2}} + (vd)_{i-\frac{1}{2}, j}^{n-\frac{1}{2}} + (vd)_{i+\frac{1}{2}, j-1}^{n-\frac{1}{2}} - (vd)_{i-\frac{1}{2}, j-1}^{n-\frac{1}{2}} \right] \end{aligned} \quad (2.12)$$

$$\begin{aligned} \left[ \frac{\partial^3 (ud)}{\partial x \partial y \partial t} \right]_{i-\frac{1}{2}, j-1}^n &= \\ \frac{1}{2\Delta x \Delta y \Delta t} & \left[ (ud)_{i, j-\frac{1}{2}}^{n+\frac{1}{2}} - (ud)_{i-1, j-\frac{1}{2}}^{n+\frac{1}{2}} - (ud)_{i, j-\frac{3}{2}}^{n+\frac{1}{2}} + (ud)_{i-1, j-\frac{3}{2}}^{n+\frac{1}{2}} \right. \\ & \left. - (ud)_{i, j-\frac{1}{2}}^{n-\frac{1}{2}} + (ud)_{i-1, j-\frac{1}{2}}^{n-\frac{1}{2}} + (ud)_{i, j-\frac{3}{2}}^{n-\frac{1}{2}} - (ud)_{i-1, j-\frac{3}{2}}^{n-\frac{1}{2}} \right] \end{aligned} \quad (2.13)$$

$$\begin{aligned} \left[ \frac{\partial^3 (vd)}{\partial y^2 \partial t} \right]_{i-\frac{1}{2}, j-1}^n &= \\ \frac{1}{2(\Delta y)^2 \Delta t} & \left[ (vd)_{i-\frac{1}{2}, j}^{n+\frac{1}{2}} - 2(vd)_{i-\frac{1}{2}, j-1}^{n+\frac{1}{2}} + (vd)_{i-\frac{1}{2}, j-2}^{n+\frac{1}{2}} \right. \\ & \left. - (vd)_{i-\frac{1}{2}, j}^{n-\frac{1}{2}} + 2(vd)_{i-\frac{1}{2}, j-1}^{n-\frac{1}{2}} - (vd)_{i-1, j-2}^{n-\frac{1}{2}} \right] \end{aligned} \quad (2.14)$$

The constant depth finite difference expressions are given in equations (4.5) and (4.6) of Ref 1. To generate the equivalent varying depth expressions, two simple changes to these equations are required. Firstly, the signs and coefficients of the terms representing the third order differentials of  $u$  and  $v$  must be changed, as explained above. Secondly, the expressions in equations (2.11) to (2.14) must be multiplied by  $(2\Delta t)$ , to achieve the correct form, and then incorporated into equations (4.5) and (4.6) of Ref 1, according to equations (2.2) and (2.3) here.

The stability and accuracy constraints of this varying depth finite difference scheme, are of a similar form to those for the constant depth scheme. The same methods are also used to impose boundary conditions around the edges of the finite difference mesh. These were discussed in detail in Reference 1.

### 2.3 Numerical results

The new finite difference scheme described in Section 2.2, includes terms which model the effect of varying depth. However, for a bed of constant depth, the new scheme should give exactly the same solution as the constant depth scheme. The new scheme was used to solve a constant depth case described in Ref 1, and identical results were obtained. This indicates that the new finite difference expressions correctly represent the relevant terms in the equations for constant depth.

All the results presented in this chapter are for a single sinusoidal input wave, the period and amplitude of which are varied for different cases. The wave is introduced along one boundary at a line of  $u$  velocity points. These may be thought of as representing a wave paddle. In all, five bathymetries were used in the various tests (see Figs 1 to 4 and 29). For those

bathymetries where this paddle extends over the entire western side of the mesh, a sponge layer absorbing boundary condition (see Ref 1) is used on the eastern side. For the wedge breakwater (see Fig 4), an additional sponge layer also covers the north side, and for the breakwater gap (see Fig 29) sponge layers cover the northern, eastern and southern sides.

### 2.3.1 Solution of linear shallow water equations

In this section, the numerical solution of equations (2.4) and (2.5) with bathymetry A (see Fig 1) is discussed. The results are shown in Figures 5 to 8 and tabulated in Table 1. The first three graphs show the variation in maximum wave amplitude with water depth, for the periods 6,10 and 15s respectively. In each case, a time history of 512 values for each of 12 positions at different depths, has been spectrally analysed, and the wave amplitude so predicted is given by the curves labelled spectral analysis. Additionally, the maximum amplitude of each time history is shown, as the curves labelled maximum amplitude. The chosen positions are indicated in the Figure 1. A similar notation is used for all the tests described in later sections.

The two remaining curves on Figures 5 to 8 are the theoretical solutions (a) and (b). These solutions do not incorporate the slope discontinuities (see Fig 1), which are a considerable complication, and so they can only give an approximate indication of wave behaviour with bathymetry A. Both solutions are derived from equations (2.4) and (2.5). Solution (a) is obtained by assuming a gentle change in depth relative to wavelength, and the following form for  $u$  and  $z$ , sinusoidal in time:

$$u = u_o(x) e^{i(\omega t - \int k dx)} \quad (2.15)$$

$$z = z_o(x) e^{i(\omega t - \int k dx)} \quad (2.16)$$

where  $\omega$  is the angular frequency, and  $k$  is the wavenumber. Substituting equations (2.15) and (2.16) into equations (2.4) and (2.5), and making some simplifying assumptions leads to the well-known relation:

$$\{z_o(x)\}^2 \sqrt{gd} = \text{constant} \quad (2.17)$$

Hence, if  $A_n$  is the wave amplitude at point  $n$ , with depth  $d_n$ , and  $A_o$  is the wave amplitude at point  $o$ , with depth  $d_o$ , then

$$A_n = \left(\frac{d_o}{d_n}\right)^{1/4} A_o \quad (2.18)$$

This equation forms the basis of solution (a); for the results here,  $A_o = 1.0$ .

If a linear variation in water depth is assumed, such that

$$d = d_o - px \quad (2.19)$$

where  $p$  is the gradient of the variation, then equations (2.4) and (2.5) can be solved exactly, by assuming a separated solution of the form:

$$z(x,t) = z_o(x) e^{i\omega t} \quad (2.20)$$

Some manipulation of equations (2.4) and (2.5), and using equations (2.19) and (2.20), leads to the equation:

$$y^2 \frac{d^2 z_o}{dy^2} + y \frac{dz_o}{dy} - \frac{4 \omega^2 y^2 z_o}{pg} = 0 \quad (2.21)$$

$$\text{where } y = \left(x - \frac{d_o}{p}\right)^{\frac{1}{2}} \quad (2.22)$$

This has the general solution

$$z_o(x) = C_1 J_o(\theta) + C_2 Y_o(\theta) \quad (2.23)$$

$$\text{where } \theta = -\frac{2w}{\sqrt{gp}} \left(\frac{d_o}{p} - x\right)^{\frac{1}{2}} \quad (2.24)$$

and  $J_o$ ,  $Y_o$  are Bessel's functions of the first and second kinds, respectively. The constants  $C_1$  and  $C_2$  can be found using the initial values of wave elevation and speed.

Equation (2.23) gives the theoretical solution (b). This includes reflections from the slope, and is an improvement over solution (a). The interference pattern caused by the reflections, which resembles a perturbation about the simpler solution, is in each graph in phase with the similar pattern in the numerical results. The 'wavelength' of the interference is the same in each case, and appears to be approximately proportional to period.

The numerical results have a relatively exaggerated interference pattern, which is probably connected to the slope discontinuities which are not modelled by the theoretical solutions. While there is generally good agreement between the numerical and theoretical values, the theoretical values are lower than the maximum amplitudes, particularly with a 6s period. Apparently, this is at least partly due to energy reflected between the slope and paddle, which causes the elevation at position 1 to be greater than 1.0.

In case these reflections become less significant after a time long enough to allow many reflections, an extended run for the 10s period was performed. However, no substantial change was found in the results.

Probably also because of the discontinuity at the toe of the slope, the variation at a point on the slope is not sinusoidal, despite the sinusoidal input wave. An indication of this behaviour can be seen from the difference between the spectral analysis and maximum amplitude values in Figs 5 to 7. Figure 8 shows that the further the point is from the toe of the slope, in the direction of decreasing depth, the more sinusoidal is the shape. Reflections at the end of this plate are prevented by the sponge layer, shown in Figure 1. This feature will be because the model, does not properly resolve waves travelling across the sudden change in depth. This effect can be expected to be ameliorated by the introduction of dispersion into the equations (see the next section).

An extra factor which makes the 6s period case less reliable, is the variation of the Courant number  $C_r$  as the water depth changes. This is defined as

$$C_r = \sqrt{gd} \frac{\Delta t}{\Delta x} \quad (2.25)$$

where  $\Delta t$ ,  $\Delta x$  are the finite difference increments in time and space respectively. The stability conditions  $C_r < 1$  and  $C_r < 1/\sqrt{2}$  apply respectively to one and two dimensional problems. Accuracy considerations also require  $C_r$  to be close to 1 or  $1/\sqrt{2}$  in the respective problems. From equation (2.25), it is clear that the accuracy condition cannot be satisfied at both large and small depths. This means that in the numerical model the wave travels slower in shallow water than in

the physical situation. Analysis shows that for a 6s period, for the situation modelled here, the error in celerity at the 2m depth is approximately 6%. The corresponding 10s period error is near 2%.

### 2.3.2 The effect of introducing dispersion

In this section, the numerical solution of equations (2.6) and (2.7) with bathymetry A (see Fig 1) is discussed. The results are shown in Figures 9 to 12, and tabulated in Table 2. The graphs show curves labelled maximum amplitude and spectral analysis, which have the same meaning as explained in Section 2.3.1. The extra complication of the third order terms in equation (2.7), means that an approach similar to theoretical solution (b) given in 2.3.1 is not practical here. Instead the theoretical solution shown in Figures 9 to 11 is derived from the solution of Laplace's equation for the velocity potential, with linearised free surface boundary conditions (see Stoker, Ref 7). This gives the dispersion relation:

$$\omega^2 = gk \tanh(kd) \quad (2.26)$$

where  $k$  is the wavenumber and  $\omega$  the angular frequency. The group velocity  $C_g$  is defined as:

$$C_g = \frac{d\omega}{dk} = \frac{C}{2} \left( 1 + \frac{2kd}{\sinh 2kd} \right) \quad (2.27)$$

where  $C$  is the celerity, and

$$C = \frac{\omega}{k} \quad (2.28)$$

Equation (2.26) can be solved using the Newton-Raphson method to give  $k$ , since  $\omega$  and  $d$  are known. Equation (2.27) then gives  $C_g$ , at the depth  $d$ .

Now equation (2.18) has the more general form

$$A_n = \left( \frac{C}{C_{gn}} \right)^{\frac{1}{2}} A_o \quad (2.29)$$

This equation applies for linear but dispersive wave motion, and for a simple shoal such as bathymetry A. If equations (2.4) and (2.5) are used, then  $C_g = (gd)^{\frac{1}{2}}$ , and equation (2.29) reduces to equation (2.18). Since  $C_g$  is known at a given depth, equation (2.29) gives the theoretical solution shown in the Figures. This cannot be expected to agree exactly with the numerical results, for three principal reasons, over and above limitations in the numerical model: (i) equation (2.26) is derived assuming constant depth, and so cannot strictly be used for varying depth. However, in practice this equation can be applied to a gently varying depth; (ii) as with the theoretical solutions of the last section, the bed slope discontinuities are not modelled; (iii) equation (2.26) differs from the dispersion relation of equations (2.6) and (2.7) - this is discussed in Ref 1. However, despite its limitations, the theoretical solution should give a good approximation to the numerical results.

It can be seen from Figs 9 to 11 that the model results are in good general agreement with the theoretical solutions. The most evident change introduced by the dispersion, is to produce a near-sinusoidal variation everywhere. This is indicated by the almost identical spectral analysis and maximum amplitude results, and also by the profiles shown in Figure 12, which display a sinusoidal variation with time at three different depths. This change is probably because dispersion spreads the energy across waves of different speeds,

and so the bed discontinuities are effectively smoothed.

Comparing Figures 9 to 11 (with dispersion) with Figures 5 to 7 (no dispersion), there are both clear similarities and differences. A similar interference pattern, due to reflections off the slope (see the last section), occurs in both sets of graphs. Again, the 6s period numerical results are furthest from the theoretical solution, and have the largest wave amplitude at the toe of the slope. The reasons for this behaviour for the 6s case will be similar to those discussed in the previous section.

### 2.3.3 The extension to two dimensions by including refraction

This section describes the numerical solution of equations (2.8) to (2.10). Two bathymetries have been used for these tests: for bathymetry B (Fig 2), results are shown in Figures 13 to 16, and for bathymetry C (Fig 3) the results are shown in Figures 17 to 19. The results are tabulated in Tables 3 and 4 respectively. In these graphs, the curves labelled spectral analysis and maximum amplitude have the same meaning as before. The theoretical solution is based on the theory of wave ray paths across the varying bed. A wave ray is defined as a line always perpendicular to the wave crest. On the assumption of conservation of energy between rays, linear theory gives:

$$A^2 C_g b = \text{constant} \quad (2.30)$$

where A is the amplitude of the wave,  $C_g$  the group velocity, and b the separation of the rays. Hence in the notation used previously:

$$A_n = \left( \frac{C_{g0} b_o}{C_{gn} b_n} \right)^{\frac{1}{2}} A_o \quad (2.31)$$

For a shoal without refraction,  $b_o = b_n$ , and equation (2.3.1) reduces to equation (2.29). The refraction of a ray obeys Snell's law, ie.

$$\frac{C_n}{C_o} = \frac{\sin \alpha_n}{\sin \alpha_o} \quad (2.32)$$

where  $\alpha_i$  is the angle between the ray path and a line perpendicular to the bed contours. As described in Section 2.3.2, the wavenumber at a given depth can be found from equation (2.2.6), which in turn gives the celerity  $c_i$  from equation (2.28). This allows calculation of the angle  $\alpha_n$  from equation (2.32), which gives the ratio  $(b_n/b_o)$ . The group velocity  $C_g$  is found as described in Section 2.3.2, and hence  $A_n$  can be found from equation (2.31). The theoretical solution given is based on this equation. It gives an approximation to the physical situation which neglects reflections, diffraction and the effects of the bed discontinuities, and is strictly only valid for constant depth, although can be applied to a gently varying depth. Further, the dispersion relation of the equations solved numerically is not identical to the dispersion relation used for the theoretical solution. However, even with these limitations, the theoretical solution can be expected to provide a good basis for verification of the results from the numerical model. It can be seen from the appropriate figures that for both of the bathymetries used in the tests, the numerical model results are in good general agreement with the theoretical values.

The results with bathymetry B will be discussed first. The positions chosen for analysis (see Fig 2) are spread throughout the basin at a range of depths. The

results at these positions are shown in Figures 13 to 15. For the 15s case results were also taken at an alternative set of points, along a line perpendicular to the contours, and starting near the lower edge of the basin. These positions are also shown in Figure 2 and the extra set of results is shown in Figure 15 labelled as points (ii). This was principally done as a check on the results taken for the original locations, to ensure that these were principally depth, rather than location, dependent. Although the resulting curve for points (ii) is smoother, the same features are apparent.

The wavelengths of the interference patterns with bathymetry B are clearly similar to those of bathymetry A, despite the differences in geometry and gradient of slope. It is likely that the large amplitudes found at position 12, near to the top wall, which are particularly pronounced for the 6s period, are partly caused by reflected energy. The boundary condition at the top wall is designed to absorb waves of normal incidence, but it allows some energy from glancing waves to reflect.

As with the straight shoal, the dispersive terms in the equations ensure an almost sinusoidal variation everywhere, which is shown in Figure 16 for three positions. However, a significant change caused by the refraction, is a reduction in wave amplitude over part of the basin, to below the input amplitude of 1.0m. This applies to the 6s and 10s periods. The reason for this is clear if two adjacent wave rays are followed across the slope. The refraction spreads the rays further apart, and so from Equation (2.30) reduces the wave amplitude. At shallower depths, the decrease in  $C_g$  more than compensates for this, and larger wave amplitudes are found.

The 15s period case deviates from the previous results with bathymetry A, by having a larger amplitude at the toe of the slope. If this large elevation is the result of constructive interference between the incoming wave and reflected waves, then it will be sensitive to both the bathymetry and the distance already travelled by the input sine wave. Comparison of Figures 1 and 2 shows that both of these geometrical factors change considerably, and so the difference in results is not surprising.

Bathymetry C has a much shallower gradient than bathymetry B (compare Figs 2 and 3), and the greatest water depth is 5m. It is therefore a less stringent test of the numerical scheme and governing equations. Figures 17 and 18 show a comparison between the numerical results of this model, and those of an alternative finite difference model, due to Copeland (Ref 2), for an input wave amplitude of 0.5m and the periods 6s and 10s, respectively.

Spectrally analysed results for the present model were not available. Copeland's model results are amplitudes averaged across a time history, whereas the results shown for the present model are maximum amplitudes. Therefore it is to be expected that the maximum amplitudes will be the greater, as is the case. The Copeland solution has a tendency, independently of period, to have a constant elevation between the depths 2.2m and 1.8m. Despite this, the solutions agree well with each other and the theoretical solution, particularly for the 6s period, which is the case considered by Copeland in his original work. It seems logical that the numerical values should exceed the theoretical ones, since the theoretical solution does not include diffraction or reflection effects, which the finite difference model does represent.

Finally, to give a general impression of the surface behaviour, isometric plots are shown in Figure 19, across part of the basin with bathymetry C, for a 15s period. The refraction effects can be clearly seen, and the variation with time is as expected, because the times 50, 100, 150 and 200s are equivalent to  $3\frac{1}{3}T$ ,  $6\frac{2}{3}T$ ,  $10T$  and  $13\frac{1}{3}T$  respectively, where T is the period.

#### 2.3.4 The introduction of non-linear terms

This Section describes the numerical solution of Equations (2.1) to (2.3). The problem has been solved in one dimension with bathymetry A, and in two dimensions with bathymetry B. For the one dimensional problem, the periods 6s and 10s were used. For the 6s period, the results are shown in Figures 20 and 23, and for the 10s period, in Figures 21 and 24: results for both periods are tabulated in Table 5. For the two dimensional problem the period 10s was used, and the results are shown in Figures 22 and 25(b), and tabulated in Table 6. Figure 25 contrasts isometric views of the 10s period solutions with bathymetries A and B. As well as showing non-linear model results, Figures 20 to 22 also show the equivalent linear spectral analysis results for comparison. The maximum amplitude curve has the same meaning as before, and the curve labelled input frequency component gives the wave amplitude associated with the input frequency. The spectral amplitude curve is calculated using the energy associated with the input frequency and its first two harmonics, while the curve labelled  $\frac{1}{2}$  (waveheight) is self-explanatory, and is included to put the maximum amplitude values into perspective. The complexity of the non-linear problem does not admit a theoretical solution.

The input wave amplitudes used to produce these results were 0.35m for the 6s period, and 0.1m for the 10s period. Such relatively small amplitudes were chosen partly because equations (2.1) to (2.3) are valid for small amplitudes ( $a \ll d$ ), and partly to ensure no breaking waves occurred, as these are outside the scope of the model. The most striking features of Figures 20 to 22, in comparison with previous linear model results, are the large values of maximum amplitude. However, this can be slightly misleading, as shown by the  $\frac{1}{2}$  (waveheight) curve, and also by Figures 23 and 24. It is clear that the shoaling non-linear wave develops a more cnoidal form at shallow depth. This behaviour has been found before both experimentally (Ref 3) and with another numerical model (Ref 4). The distinctive wave shape, with sharp peaks and shallow troughs, is caused by the interaction of the input wave with its excited harmonics. Figure 23 is for the 6s period, and shows that the wave has settled to a steady shape in the 2m depth area, which is evident also in the constant maximum amplitude values for the same region in Figure 20. In contrast, Figure 24 shows that the 10s period wave changes form in this area, and this is reflected in the increasing amplitude for this region shown in Figure 21. It is likely that a much longer area at the 2m depth would also allow the 10s period wave to settle.

The linear spectral analysis curve has been included in Figures 20 to 22, for comparison with the spectral amplitude results of the non-linear model. Identical input waves were used in each case, and so very similar curves can be expected. In fact, the spectral amplitude curve is consistently slightly larger, particularly in the more shallow water. This phenomenon is supported by the work of Elgar and Guza (Ref 3), who have compared experimental results with

those of both linear and non-linear numerical models. They found that the linear model under-predicts, while the non-linear model over-predicts the energy levels at higher frequencies, particularly in shallow water. They suggest this fault in the non-linear model may be due to the condition  $a \ll d$  not being satisfied.

An interesting experimental result (Ref 3), which the non-linear model predicts for a 10s period with bathymetry A (the relevant results are shown in Figure 21), is the transference of energy from the input frequency to one of its harmonics. This is evidenced by the reduction in energy, along the 2m plateau, of energy associated with the input frequency, with a corresponding increase in the total spectral amplitude. Additionally, experimental tests with a mildly sloping beach (Ref 3), have shown that the lowest frequency waves are almost completely reflected, while the highest frequency waves are primarily progressive. This helps to explain waveheights at the toe of the slope which are greater than the input waveheight.

The inclusion of the linear spectral analysis curves in Figures 20 to 22, shows that the wavelength of the interference pattern caused by the incoming and reflected waves, is unchanged by the introduction of the non-linear behaviour, for both bathymetries A and B. The pattern evidently depends principally on the bathymetry.

Figure 25(a), which is for the 10s period wave with bathymetry A, demonstrates the development of a cnoidal wave, with sharp peaks and shallow troughs, as the wave shoals. Figure 25(b) shows the equivalent situation for bathymetry B, where the wave both shoals and refracts. The small elevations at the far end of

the basin in each case, are because of the sponge layer boundary condition there.

### 2.3.5 Diffraction from the corner of a "wedge" breakwater

In this Section, the ability of the numerical scheme to model diffraction is discussed. Bathymetry D, shown in Figure 4, has been used, which is a modified version of bathymetry C. A wedge has been introduced across 2/3 of the open boundary, as shown, and so diffraction can be expected from its corner. Positions chosen for analysis are situated in the shadow of the wedge (numbers 1, 2 and 3), at the end of the channel beside the wedge (number 4), and following the approximate path of a ray across the bed (numbers 5 to 12), as shown in Figure 4. An extra set of thirteen points have also been used, to study the behaviour along a line between positions 4 and 5, and at intermediate points along the ray path to clarify the interference effect due to reflected energy from the slope. These extra points are not shown in Figure 4, but if their positions are required, they can easily be found using Figure 26.

As before, a sponge layer at the end of the basin is designed to absorb the waves incident there. This test was carried out with a 10s period input wave, of amplitude 0.1m, for both the linear and non-linear cases, and the results are shown in Figures 26 to 28, and tabulated in Table 7.

The titles of the curves shown in Figure 26 have the same meaning as explained in Section 2.3.4. They give a comparison between the linear and non-linear results. The non-linear spectral amplitude curve is identical to the linear spectral analysis curve, therefore both are plotted as one. As in the previous

section, the  $\frac{1}{2}$  (waveheight) curve puts the maximum amplitudes into perspective. Figure 27 is also useful in this respect, as it shows the non-linear wave shape at position 12. It is plotted with the sinusoidal linear solution, to show the effect of the non-linear terms.

As expected, the amplitudes at Positions 1, 2 and 3, in the shadow of the wedge, are small. This can be seen in Figure 26, and also in Figure 28, which shows elevations across most of the basin at four different times, for the non-linear case. While Figure 28 is effective at showing the general features of the flow, in particular the diffraction and refraction, Figure 26 is more effective at showing the variation in amplitude across the basin. The drop in amplitude between positions 4 and 5, due to diffraction at the wedge corner, can be seen. The toe of the slope affects the flow in the constant depth area in front of it, causing the minimum amplitude to occur at a position nearly 20m in front of the toe. Also clear is the now familiar interference pattern, due to reflected energy, as the wave shoals.

#### 2.3.6 Diffraction by a breakwater gap, with constant water depth

The work described in this section was conducted as a further test of the numerical model's ability to model diffraction, and also to ensure that a sponge layer introduced on the southern boundary was functioning correctly. The linearised, constant depth form of equations (2.1) to (2.3) was solved, and this allows comparison with the earlier theoretical work of Montefusco (Ref 6) and Smallman (Ref 5).

The solution domain is shown in Figure 29. Waves of period 10s are normally incident on a breakwater gap

to the west, which opens onto an area of constant depth 10m. The northern, eastern and southern walls of the harbour are lined by a sponge layer 20 cells wide, where the cell width is 5m. The layer is thus 100m wide, which equals approximately one wavelength of the incident wave. For comparison with the two theoretical solutions, the gap width was chosen as 1.75 wavelengths. The twenty analysis positions shown in the figure were chosen to correspond with the theoretical solution positions.

Figure 30 shows a comparison between the spectrally analysed results of the present model, and the theoretical solutions. These are also tabulated in Table 8. Overall, the agreement is good, indicating that diffraction into the breakwater shadow is well represented, and that the sponge layers are acting to absorb wave energy. Further, the solution was found to be symmetric about the centre line and therefore the southern sponge layer must be operating correctly. Figure 31 shows that the sinusoidal behaviour of the input wave, is reproduced within the harbour, as to be expected for a linear solution.

#### 2.4 Summary

The numerical model for a solution of the Boussinesq equation in water of constant depth, has been extended to include the effects of depth variation. This required the introduction of new terms in the finite difference scheme representing the governing equations.

The new finite difference scheme has been tested for a variety of bathymetries and harbour geometries. Good agreement has been found with both theoretical solutions and another finite difference model, for linear shoaling and refraction. For the full non-linear scheme, although no other theoretical

solutions or suitable numerical results are available, good qualitative agreement has been found with experimental results.

Additional tests carried out to examine diffraction, using a wedge breakwater, and also a breakwater gap, produced good results.

### 3 RANDOM INCIDENT WAVES

#### 3.1 Background

It is important that a numerical model of wave disturbance in harbours should represent as far as possible the wave conditions which occur in nature. In the approaches to a harbour waves will be random and multi-directional (short crested), and the aim should be to reproduce this in harbour wave disturbance models. Physical models have already made significant progress towards this end, see Bowers (Ref 8); numerical models are, in general, still some distance away. However, having considered both unidirectional regular and bichromatic wave trains (see Ref 1) the next stage in the development of the present model is to represent unidirectional random wave input. This process is described in the following parts of this chapter.

Before proceeding to the details of the implementation of random waves, it is worth restating that one significant feature of the present model is its ability to represent the propagation of set down beneath wave groups. This was demonstrated for a system consisting of sine waves of two frequencies and its associated set down in Smallman et al (Ref 1). This is the simplest example of set down beneath wave groups, but it should be recalled that in deriving the boundary conditions for this case, the second order

terms needed to be specified so that the correct set down behaviour is achieved, and no spurious long waves are introduced at the boundary. The same holds true for the more complex situation of set down beneath a random wave train. Here set down will occur between all the different frequency components of the wave spectrum. The second order terms which are required at the boundary for the case are discussed in section 3.2. A description of the tests used to verify the model results is given in section 3.3.

### 3.2 Boundary conditions

The first order elevation of a unidirectional random wave train at position  $x$  and time  $t$  may be written in discrete form as,

$$\eta^{(1)}(x,t) = \sum_{i=1}^n a_i \cos(\omega_i t - k_i x + \epsilon_i) \quad (3.1)$$

here  $a_i$ ,  $\omega_i$  and  $k_i$  are the amplitude, radian frequency and wave number associated with the discrete frequencies  $f_i$ ,  $i=1,2,\dots,n$ , and the  $\epsilon_i$  are random phase terms. The discrete frequencies can be defined in terms of the frequency increment  $\Delta f$  as,

$$f_i = \Delta f (i - \frac{1}{2}), \quad i = 1, 2, \dots, n.$$

The amplitudes  $a_i$  can be written in terms of the energy frequency spectrum,

$$a_i^2 = 2 \int_{f_i - \Delta f/2}^{f_i + \Delta f/2} S(f) df,$$

which can be approximated as,

$$a_i^2 \approx 2.S(f_i).\Delta f.$$

The discrete wave numbers  $k_i$  are given by,

$$k_i^2 = \frac{\omega_i^2}{\left(gd - \frac{\omega_i^2 d^2}{3}\right)}$$

where

$$\omega_i = 2\pi f_i, \quad i = 1, \dots, n.$$

For the Boussinesq equations the characteristics of the set down can be determined by examining the one dimensional form of the differential equations (2.1) and (2.2). By expanding the various terms in these equations to second order and by use of equation (3.1), it can be shown that the second order elevation which includes the set down terms is,

$$\eta^{(2)}(x, t) = \sum_{i=j+1}^n \sum_{j=1}^{n-1} A_{ij} \cos(\omega_{ij} t - k_{ij} x + \epsilon_{ij}) \quad (3.2)$$

where

$$\begin{aligned} \omega_{ij} &= \omega_i - \omega_j \\ k_{ij} &= k_i - k_j \\ \text{and } \epsilon_{ij} &= \epsilon_i - \epsilon_j. \end{aligned}$$

The amplitudes  $A_{ij}$  are given by,

$$A_{ij} = \frac{k_{ij}}{\omega_{ij}} d U_{ij} + \frac{a_i a_j}{2d} \frac{k_{ij}}{\omega_{ij}} \left( \frac{\omega_i}{k_i} + \frac{\omega_j}{k_j} \right), \quad j=1 \text{ to } n-1, i=j, n$$

where

$$U_{ij} = \frac{a_i a_j k_{ij}}{2d} \frac{\left( \frac{\omega_{ij}}{d k_i k_j} + g k_{ij} \left( \frac{\omega_i}{k_i} / \frac{\omega_j}{k_j} \right) \right)}{\omega_{ij}^2 \left( 1 + \frac{k_{ij}^2 d^2}{3} \right) - g d k_{ij}^2}, \quad j=1 \text{ to } n-1, i=j, n \quad (3.3)$$

Equation (3.2), which was derived from the Boussinesq equations differs from that which is derived using Laplace's equation and free surface boundary conditions taken to second order. In this case the expression for the second order elevation is,

$$\eta^{(2)}(x,t) = \sum_{i=j+1}^n \sum_{j=1}^{n-1} \bar{A}_{ij} \cos(\omega_{ij}t - k_{ij}x + \epsilon_{ij}) \quad (3.4)$$

where

$$\bar{A}_{ij} = a_i a_j \left[ \bar{\gamma}_{ij} + \frac{1}{2} (k_i \tanh k_i d + k_j \tanh k_j d) \frac{k_i k_j g}{2\omega_i \omega_j} (1 + \tanh k_i d \tanh k_j d) \right]$$

and

$$\bar{\gamma}_{ij} = \frac{\omega_{ij} g}{2} \frac{\left[ \frac{2k_i k_j}{\omega_i \omega_j} \omega_{ij} (1 + \tanh k_i d \tanh k_j d) + \frac{k_i^2}{\omega_i \cosh k_i d} \frac{k_j^2}{\omega_j \cosh k_j d} \right]}{(\omega_{ij}^2 - g k_{ij} \tanh k_{ij} d)}$$

The derivation of equation (3.4) is given in Spencer (Ref 9).

Equation (3.2) and (3.4) cannot be expected to yield the same values as they arise from different equations. However, because the Boussinesq equation dispersion relation is a reasonable approximation to the dispersion relation derived in potential theory, we can expect the set down amplitude arising from equation (3.2) to be a reasonable approximation to those given by equation (3.4). The approximation given by equation (3.2) improves as the water depth decreases.

### 3.3 Implementation and verification

The boundary conditions for the numerical model are supplied in terms of the elevation, and corresponding  $u$  velocity at a series of grid points at the edge of the model. These grid points can be thought of as corresponding to a wave paddle, with the elevations and velocities being specified in terms of a time series at  $x=0$  which generated using equations (3.1) and (3.2) for a given wave spectrum.

In order to verify that the model was working correctly two test cases were run, and their results compared with the expected theoretical values of amplitude or spectral density for both the set down and primary wave components. For both tests the mathematical model was set up to represent a wave flume of 10m depth, with the input wave being specified at one end and a sponge layer boundary condition at the other.

The first test which was carried out used an incident spectrum which consisted of waves at two frequencies only. In this case the group of waves (and hence the set down) occur with a frequency equal to the difference between the two primary frequencies.

This type of test will provide a clear indication of the model's performance as substantial amounts of energy should only be present in three frequency components at all locations in a constant depth flume, these will correspond to the two primary frequencies and the set down frequency. Similar tests were carried out in Ref 1 using two sine waves and the associated set down to provide input to the model, rather than the wave spectrum representing this combination which is used here.

The characteristics of the input spectrum for the regular wave group test were as follows:

Frequency (Hz)	Spectral density ( $m^2s$ )	Amplitude (m)
0.10	79.98	0.5
0.07	28.79	0.3

The set down component calculated by the numerical model was at a frequency of 0.03Hz with an amplitude of 0.075m. The mathematical model was run using a 5m mesh with a time step of 0.34s, giving a Courant number of 0.67. Using  $\Delta x=5m$  gives approximately 20 points to the shortest primary wavelength. Time series of the surface elevations were collected during the model run at a number of positions along the flume, and a spectral analysis carried out to obtain the amplitudes of the frequency components at these positions. The results from this test are summarised in Table 9.

It can be expected that if the wave group is propagating correctly in a flume of constant depth then the amplitude of each of the frequency components should remain constant throughout the length of the flume. It can be seen from Table 9 that the amplitude of the set down is within 8% of its expected value at all positions along the flume. This confirms that the model is both generating the correct set down component from the primary wave spectrum and propagating it accurately throughout the model area. An isometric view of the surface elevation for this test at various times during the model run is shown in Figure 32.

The second test which was carried out to test the spectral input used as input a Pierson-Moskowitz spectrum; this should provide a more stringent test of

the models capability to propagate correctly a random wave train with its associated set down component. In this case the Pierson Moskowitz spectrum which was used, see Figure 33, was characterised as having a peak period of 10s. The selection of space and time steps for the numerical model with random wave input is less straightforward than for either a sine wave or a bichromatic wave input. Care needs to be taken that the space step is selected so that the wavelengths corresponding to the full range of frequency components are accurately resolved. For the primary wave spectrum given here there is significant energy in the range 0.05Hz to 0.2Hz, and we therefore need to ensure that the space step is selected so that there are sufficient points per wavelength for wave periods of around 5s (frequency 0.2Hz). A space step  $\Delta x = 5\text{m}$ , will give approximately 10 points per wavelength for the 5s component in 10m depth, and 20 points per wavelength for a wave period 10s.

Having selected the space step the numerical model is constrained by the Courant stability condition, which for the two-dimensional case is,

$$C_r = \frac{(gd)^{\frac{1}{2}} \Delta t}{\Delta x} < 1/\sqrt{2} \quad ,$$

for its choice of time step. A time step of  $\Delta t = 0.34\text{s}$  satisfies this constraint, if the one-dimensional stability criterion  $C_r < 1$  was used the time step could be slightly longer. However, whilst the present test is one-dimensional, the model will in practical situations be required to satisfy the two-dimensional conditions.

Before discussing the model results, it is appropriate to comment on the constraints which are imposed by the

method of analysis which is used. The spectral analysis procedure used in this model is the same as that employed in physical model studies. This method analysis the surface elevation from the model at each point of interest and calculates the spectral density at certain discrete frequency intervals. From the spectral density the significant wave height, zero crossing period and amplitude of the waves at that point an be derived. The discrete frequency intervals are calculated from the length of the wave record and a smoothing parameter which combines energy for neighbouring frequency bands. The number of surface elevations in a time history must be a value of  $2^n$  to facilitate the fast Fourier transform method (see Ref 10) which is used. Typically in physical models 2048 or 4096 points are analysed. For the present numerical model either 512 or 1024 points are normally used, as it becomes expensive, in terms of computer time, to run the model for a larger number of time steps. The value of the time step in a physical model is selected so that the discrete frequency intervals in the spectral analysis cover the important range of frequencies of the wave spectrum used in the physical model test. It is not possible to do this for the numerical model as the time step is fixed by the stability and accuracy considerations.

As a result of this the number of discrete bands in the spectral analysis covering the important frequencies will be much lower than for the physical model case, leading to a loss of resolution in the calculation of spectral density. In addition, the smaller number of time step used (say 1024) means that the record length is shorter than for the equivalent physical model test, and thus fewer waves are being analysed.

With all these points in mind it is clear that determining the spectral density of several individual set down components from the numerical model results will not be straightforward, as the relevant range of frequencies will be covered by a small number of frequency bands, and the record analysed will be fairly short. However, it can be demonstrated that the model does represent set down beneath random wave groups. This is done by comparing the spectral density at frequencies below 0.04Hz at various positions along the numerical model wave flume with their theoretical values calculated using expression (A4) from Appendix 1.

Prior to making this comparison some comment should be made about the expected value of the set down spectral density for both the Boussinesq equations and Laplace's equation (see section 3.2). For frequencies below 0.04Hz the set down spectra using both expressions are shown in Figure 33. It can be seen that for this case the spectral density of the set down from the Boussinesq equations is within 15% of the value calculated using Laplace's equation. It has been shown in Reference 1 that the approximation derived using the Boussinesq equations improves as the water depth decreases.

The results from the numerical model test carried out using the input Spectrum shown in Figure 33 are displayed in Figure 34 as the spectra up to 0.04Hz at various distances (d) from the paddle along the wave flume. As can be seen, allowing sufficient smoothing in the Fourier analysis of the wave elevations results in their being only four points covering the range of interest. (The model was run for 2000 time steps and the last 1024 points analysed.) The results in Figure 34 demonstrate that the Boussinesq model does give a reasonable approximation of the set down

spectral shape, and has the correct spectral density at the lower frequencies where it will be of most importance.

At frequencies between 0.015Hz the agreement between the predicted and expected values is not as good, with the predicted spectral densities being lower than the expected values. This is in contrast to the results shown in Table 9 for regular wave groups where the agreement of the model results with the expected values of amplitude was good at the primary frequencies (0.10Hz and 0.07Hz) and at the set down frequency (0.03Hz).

The agreement between the calculated and expected spectral densities is better nearer the wave paddle. It is likely that at distances  $d = 362.5\text{m}$  and  $d = 462.5\text{m}$  that there will be some low frequency interference from reflections from the sponge layer boundary condition. Such reflections are also known to occur in physical models where the shingle beaches do not absorb all the long period wave energy. It is possible that better agreement could be achieved if more elevations were analysed, say 2048, but in practise the cost of running the model would be prohibitive.

In addition to the comparison shown in Figure 34 the spectral densities at the peak period of the primary spectrum were also examined. It can be seen from Table 10 that at all locations along the flume the energy at the peak frequency remained within 10% of its expected value. To give a better impression of the surface profile for a random wave input an isometric view is given in Figure 35.

In summary, the numerical model solving the Boussinesq equations has been successfully modified to allow random wave input. From the results given in this

section we conclude that the numerical model gives a reasonable representation of set down effects for a random wave train. However, further tests will need to be carried out to examine these effects for the varying depth case, where comparison with physical model results will allow the numerical model to be assessed more rigourously. In addition, further consideration will need to be given to the method of analysis of the numerical model results with respect to time step constraints in stability, accuracy and running costs.

## 4 CONCLUSIONS AND RECOMMENDATIONS

### 4.1 Conclusions

The mathematical model which provided a numerical solution to the Boussinesq equations in water of constant depth (see Ref 1) has been developed further to include varying depth terms and unidirectional random wave input. The model has been shown to provide a good representation of the effects of refraction and shoaling, and diffraction by breakwaters in varying depth. Comparisons between the model results and theoretical solutions were good for the linear case, and the non-linear results appear to be promising. The model also successfully reproduced the effects of set down beneath a random wave train in water of constant depth.

### 4.2 Recommendations

In order to test fully the non-linear aspects of the mathematical model we require data against which to compare the results. For the varying depth case the governing non-linear equations do not admit an analytical solution. It is therefore recommended that a series of physical model tests are carried out to

provide comprehensive data against which to validate the numerical model.

To further develop the numerical model to allow more realistic harbour layouts to be represented it is recommended that:

- a) Boundary conditions for the model should be fully investigated; in particular consideration needs to be given to representing partially reflecting structures, (eg rubble mound breakwaters).
- b) Implementation of multi directional incident waves in the model should be investigated.
- c) Extension of the present equations to include energy losses due to seabed friction should be examined.
- d) Some thought should be given to the future inclusion of the effects of tidal currents in the mathematical model.

## 5 ACKNOWLEDGEMENTS

The research described in this report was carried out by members of Dr S W Huntingtons Maritime Engineering Department. The authors would like to thank colleagues in the department for their helpful discussions. In particular, acknowledgement is due to Dr E C Bowers for the development of the basic theory given in section 3.2, and for many of the ideas behind this research. The authors would also like to thank Dr A J Cooper of the Tidal Engineering Department for his help and advice.

6 REFERENCES

1. Smallman, J V, Matsoukis, P F, Cooper, A J and Bowers, E C. The development of a numerical model for the solution of the Boussinesq equation for shallow water waves - Constant depth case. Hydraulics Research Report No. SR 137, August 1987.
2. Copeland, G J M. A numerical model for the propagation of short gravity waves and the resulting circulation around nearshore structures. PhD Thesis, University of Liverpool, February 1985.
3. Elgar, S and Guza, R T. Shoaling gravity waves: comparisons between field observations, linear theory, and a non-linear model. *J Fluid Mech* 158 47-70, 1985.
4. Madsen, P A and Warren, I R. Performance of a numerical short-wave model. *Coastal Engineering*, 8 73-93, 1984.
5. Smallman, J V. Wave action at a series of offshore breakwaters: a mathematical model of wave diffraction and overtopping. Report No. SR 59.
6. Montefusco, L. Sea waves diffraction through a break in a rectilinear wall. XI Convegno di Idraulics and Costruzioni Idrauliche, Genoa, October 1968 (In Italian).
7. Stoker, J J. *Water waves*. Interscience, 1966.
8. Bowers E C. Short crested seas in harbour modelling Hydraulics Research Report SR 41. November 1987.

9. Spencer J M A. Second order waves in long crested random sea states. Hydraulics Research Report IT 257. October 1983.
  
10. Thompson D M and Gilbert G. The fast Fourier transform with applications to spectral and cross spectral analysis. Hydraulics Research Report INT 100. December 1971.

**TABLES.**



TABLE 1 Results with bathymetry A: numerical solution of equations (2.4) and (2.5)

DEPTH (m) Position	PERIOD T=6s		PERIOD T=10s		PERIOD T=15s		Theoretical solution (a)
	Numerical model	Theoretical solution (b)	Numerical model	Theoretical solution (b)	Numerical model	Theoretical solution (b)	
(1) 10.0	1.08	1.00	0.94	1.00	1.00	1.00	1.00
(2) 8.6	1.17	1.04	1.01	1.02	1.03	1.02	1.04
(3) 6.6	1.25	1.12	1.03	1.11	1.22	1.13	1.11
(4) 5.8	1.21	1.15	1.07	1.12	1.21	1.17	1.15
(5) 5.0	1.37	1.19	1.19	1.19	1.17	1.19	1.19
(6) 4.2	1.33	1.25	1.22	1.26	1.22	1.22	1.24
(7) 3.4	1.53	1.32	1.21	1.30	1.41	1.29	1.31
(8) 2.6	1.59	1.38	1.42	1.40	1.55	1.42	1.40
(9) 2.0	1.77	1.51	1.46	1.52	1.54	1.52	1.49
(10) 2.0	1.77	-	1.47	-	1.56	-	-
(11) 2.0	1.77	-	1.47	-	1.60	-	-
(12) 2.0	1.77	-	1.47	-	1.54	-	-

(Input wave amplitude = 1.00m)

Notes

- (i) The numerical solution values are the result of spectral analysis of a time history
- (ii) The calculation of the theoretical solution values (a) and (b) is explained in Section 2.3.1
- (iii) The location of each position given in this table is shown in Figure 1
- (iv) The results are shown graphically in Figures 5-7

TABLE 2 Results with bathymetry A: numerical solution of equations (2.6) and (2.7)

DEPTH (m) Position	PERIOD T=6s		PERIOD T=10s		PERIOD T=15s	
	Numerical solution	Theoretical solution	Numerical solution	Theoretical solution	Numerical solution	Theoretical solution
(1) 10.0	1.02	1.00	0.99	1.00	0.99	1.00
(2) 8.6	1.02	1.00	0.99	1.03	0.99	1.03
(3) 6.6	1.04	1.01	1.03	1.07	1.19	1.09
(4) 5.8	1.02	1.02	1.03	1.09	1.17	1.12
(5) 5.0	1.07	1.03	1.14	1.13	1.11	1.16
(6) 4.2	1.05	1.05	1.17	1.17	1.15	1.21
(7) 3.4	1.16	1.08	1.15	1.22	1.33	1.27
(8) 2.6	1.17	1.13	1.34	1.30	1.47	1.36
(9) 2.0	1.29	1.19	1.37	1.37	1.45	1.44
(10) 2.0	1.29	-	1.37	-	1.47	-
(11) 2.0	1.29	-	1.38	-	1.50	-
(12) 2.0	1.29	-	1.38	-	1.45	-

(Input wave amplitude = 1.00m)

Notes

- (i) The numerical solution values are the result of spectral analysis of a time history
- (ii) The calculation of the theoretical solution values is explained in Section 2.3.2
- (iii) The location of each position given in this table is shown in Figure 1
- (iv) The results are shown graphically in Figures 9-11

TABLE 3 Results with bathymetry A: numerical solution of equations (2.8) and (2.10)

DEPTH (m) Position	PERIOD T=6s		PERIOD T=10s		PERIOD T=15s	
	Numerical solution	Theoretical solution	Numerical solution	Theoretical solution	Numerical solution	Theoretical solution
(1) 10.0	1.02	1.00	1.01	1.00	1.03	1.00
(2) 8.6	1.00	1.00	1.01	1.00	1.09	1.01
(3) 6.6	0.99	1.00	0.98	1.01	1.12	1.02
(4) 5.8	1.01	1.00	0.98	1.02	1.13	1.03
(5) 5.0	0.96	1.01	1.00	1.04	1.14	1.06
(6) 4.2	0.97	1.01	1.05	1.05	1.07	1.08
(7) 3.4	0.99	1.02	1.10	1.06	1.07	1.09
(8) 2.6	0.98	1.02	1.06	1.09	1.09	1.12
(9) 2.0	0.98	1.03	1.11	1.10	1.14	1.13
(10) 2.0	1.01	1.05	1.12	1.16	1.27	1.19
(11) 2.0	1.05	1.10	1.29	1.24	1.47	1.28
(12) 2.0	1.22	1.14	1.46	1.30	1.46	1.36

(Input wave amplitude = 1.00m)

Notes

- (i) The 15s period numerical solution results given in this table, are shown in Figure 15 as points (i). They are determined by spectral analysis of a time history
- (ii) The calculation of the theoretical solution values is explained in Section 2.3.3
- (iii) The location of each position given in the table is shown in Figure 2
- (iv) The results are shown graphically in Figures 13-15

**TABLE 4 Results with bathymetry C: numerical solution of equations (2.8) and (2.10)**

DEPTH (m) Position	PERIOD T=6s			PERIOD T=15s		
	Numerical solution	Copeland solution	Theoretical solution	Numerical solution	Copeland solution	Theoretical solution
(1) 5.00	0.49	-	0.50			
(1a) 5.00				0.50	-	0.50
(2) 4.53	0.51	0.50	0.50	0.52	0.50	0.51
(3) 4.15	0.52	0.51	0.51	0.54	0.51	0.52
(4) 3.85	0.52	0.52	0.51	0.53	0.52	0.52
(5) 3.45	0.52	0.52	0.52	0.54	0.52	0.53
(6) 3.05	0.53	0.53	0.52	0.53	0.53	0.54
(7) 2.65	0.56	0.54	0.53	0.57	0.56	0.56
(8) 2.15	0.57	0.57	0.55	0.59	0.58	0.58
(9) 1.75	0.60	0.57	0.57	0.64	0.57	0.61
(10) 1.35	0.63	0.63	0.60	0.68	0.62	0.64
(11) 1.00	0.69	0.66	0.64	-	-	-
(11a) 1.00	-	-	-	0.75	0.68	-
(12) 1.00	0.69	0.66	-	-	-	-
(12a) 1.00	-	-	-	0.72	0.67	-

(Input wave amplitude = 0.50m)

Notes

- (i) The numerical solution values are each the maximum of a time history
- (ii) The Copeland solution values are from the numerical model (described in Ref 2) and are averaged across time (see Section 2.3.3)
- (iii) The calculation of the 'theoretical' values is explained in Section 2.3.3
- (iv) The location of each position given in the table is shown in Figure 3
- (v) These results are shown graphically in Figures 17 & 18

**TABLE 5** The non-linear problem with bathymetry A: numerical solution of one dimensional form of equations (2.1) - (2.3)

Position	DEPTH (m)	PERIOD T=6s		PERIOD T=15s	
		Max Elevation	Spectral Amplitude	Max Elevation	Spectral Amplitude
(1)	10.0	0.38	0.36	0.10	0.10
(2)	8.6	0.38	0.36	0.11	0.10
(3)	6.6	0.40	0.37	0.11	0.10
(4)	5.8	0.39	0.36	0.11	0.10
(5)	5.0	0.42	0.37	0.12	0.10
(6)	4.2	0.42	0.36	0.12	0.11
(7)	3.4	0.48	0.41	0.12	0.12
(8)	2.6	0.51	0.42	0.14	0.12
(9)	2.0	0.57	0.47	0.16	0.13
(10)	2.0	0.58	0.47	0.17	0.14
(11)	2.0	0.58	0.47	0.18	0.14
(12)	2.0	0.58	0.47	0.20	0.14

(Input wave amplitude = 0.35m)                      (Input wave amplitude = 0.1m)

Notes

- (i) The spectral amplitude values incorporate the energy associated with the fundamental frequency ( $\cong 1/T$ ) and its first two harmonics ( $2/T$  and  $3/T$ )
- (ii) The location of each position given in the table is shown in Figure 1
- (iii) The results are shown graphically in Figures 20 & 21

**TABLE 6** The non-linear problem with bathymetry B: numerical solution of equations (2.1) - (2.3)

Position	DEPTH (m)	PERIOD T = 10s	
		Max Elevation	Spectral Amplitude
(1)	10.00	0.11	0.10
(2)	9.50	0.11	0.10
(3)	8.85	0.10	0.97
(4)	8.40	0.11	0.98
(5)	7.25	0.11	0.10
(6)	6.55	0.11	0.11
(7)	6.10	0.12	0.11
(8)	5.38	0.12	0.11
(9)	4.98	0.12	0.11
(10)	3.85	0.12	0.11
(11)	2.75	0.14	0.13
(12)	2.15	0.18	0.15

(Input wave amplitude = 0.1m)

Notes

- (i) The spectral amplitude values incorporate the energy associated with the fundamental frequency ( $\cong 1/T$ ) and its first two harmonics ( $2/T$  and  $3/T$ )
- (ii) The location of each position given in the table is shown in Figure 2
- (iii) The results are shown graphically in Figure 22

**TABLE 7 Results with bathymetry D: numerical solution of the linear (equations (2.8) - (2.10)) and non-linear (equations (2.1) - (2.3)) problems.**

Position	DEPTH (m)	Spectral Amplitude = linear spectral analysis	Maximum Elevation - non linear	$\frac{1}{2}$ (Wave Height) - non-linear
(1)	5.00	0.02	0.03	0.02
(2)	4.00	0.02	0.03	0.02
(3)	3.03	0.02	0.03	0.02
(4)	5.00	0.11	0.12	0.11
(5)	5.00	0.07	0.08	0.07
(6)	4.35	0.07	0.08	0.07
(7)	3.65	0.07	0.08	0.07
(8)	3.05	0.07	0.08	0.07
(9)	2.45	0.07	0.08	0.08
(10)	1.78	0.08	0.09	0.08
(11)	1.28	0.08	0.10	0.09
(12)	1.00	0.09	0.13	0.10

(Input wave amplitude = 0.1m)

Notes

- (i) The spectral amplitude values incorporate the energy associated with the fundamental frequency ( $= 1/T$ ) and its first two harmonics ( $2/T$  and  $3/T$ ). The linear results are identical to the non-linear.
- (ii) Points (1) to (3) are in the shadow of the wedge. The locations of all the positions are shown in Fig 4.
- (iii) The results are shown graphically in Fig 26.

**TABLE 8 Results for the breakwater gap problem, and comparison with theoretical results**

Position	Wave Amplitude (m)		
	Present Model (spectral analysis)	Montefusco (Ref 6)	Smallman (Ref 5)
1	1.36	1.20	1.10
2	1.27	1.13	1.00
3	1.18	1.07	0.90
4	1.08	0.99	0.80
5	0.99	0.89	0.70
6	1.10	1.00	1.00
7	1.01	0.92	0.90
8	0.74	0.83	0.80
9	0.67	0.75	0.70
10	0.58	0.67	0.60
11	0.55	0.58	0.50
12	0.52	0.49	0.40
13	0.49	0.46	0.30
14	0.46	0.43	0.20
15	0.80	0.79	0.70
16	0.59	0.64	0.60
17	0.43	0.52	0.50
18	0.27	0.36	0.40
19	0.16	0.29	0.30
20	0.13	0.24	0.20

Notes

- (i) The gap configuration is shown in Figure 29. The depth everywhere is 10m, the incident wave period is 10s, and the gap width is therefore 1.75 wavelengths
- (ii) The Montefusco results were obtained by interpolating between given values.

TABLE 9 Random wave tests for regular wave groups with primary frequencies 0.07Hz and 0.10z. Water depth 10m,  $\Delta x = 5m$ ,  $\Delta t = 0.34s$ . Expected wave amplitudes are 0.075m at  $f = 0.03Hz$  0.3m at  $f = 0.07Hz$  and 0.5m at  $f = 0.10Hz$

<u>Dist from paddle (m)</u>	<u>Amplitude (m) at</u>		
	<u>f = 0.03Hz</u>	<u>f = 0.07Hz</u>	<u>f = 0.10Hz</u>
2.5	0.073	0.33	0.47
62.5	0.071	0.33	0.44
112.5	0.076	0.32	0.45
162.5	0.073	0.30	0.46
212.5	0.077	0.32	0.47
262.5	0.079	0.34	0.47
312.5	0.076	0.32	0.46
362.5	0.070	0.31	0.46
412.5	0.075	0.30	0.48
462.5	0.078	0.31	0.48
512.5	0.070	0.31	0.47
562.5	0.081	0.33	0.47

TABLE 10 Random wave tests tests with Pierson Moskowitz spectrum  $T_p = 10s$   
 Water depth = 10m,  $\Delta x = 5m$ ,  $\Delta t = 0.34s$ , 1024 time steps analysed,  
 $\Delta f =$

<u>Dist from</u> <u>paddle (m)</u>	<u>Primary component at 0.109Hz</u>	
	<u>S(f) (m<sup>2</sup>s)</u>	<u>a(m)</u>
2.5	14.4	0.58
62.5	13.1	0.55
112.5	13.3	0.55
162.5	14.5	0.58
212.5	16.7	0.62
262.5	13.9	0.56
312.5	15.7	0.60
362.5	16.5	0.61
412.5	16.7	0.62
462.5	16.0	0.61
512.5	13.9	0.57
562.5	15.8	0.60
Expected value	14.1	0.57

**FIGURES.**



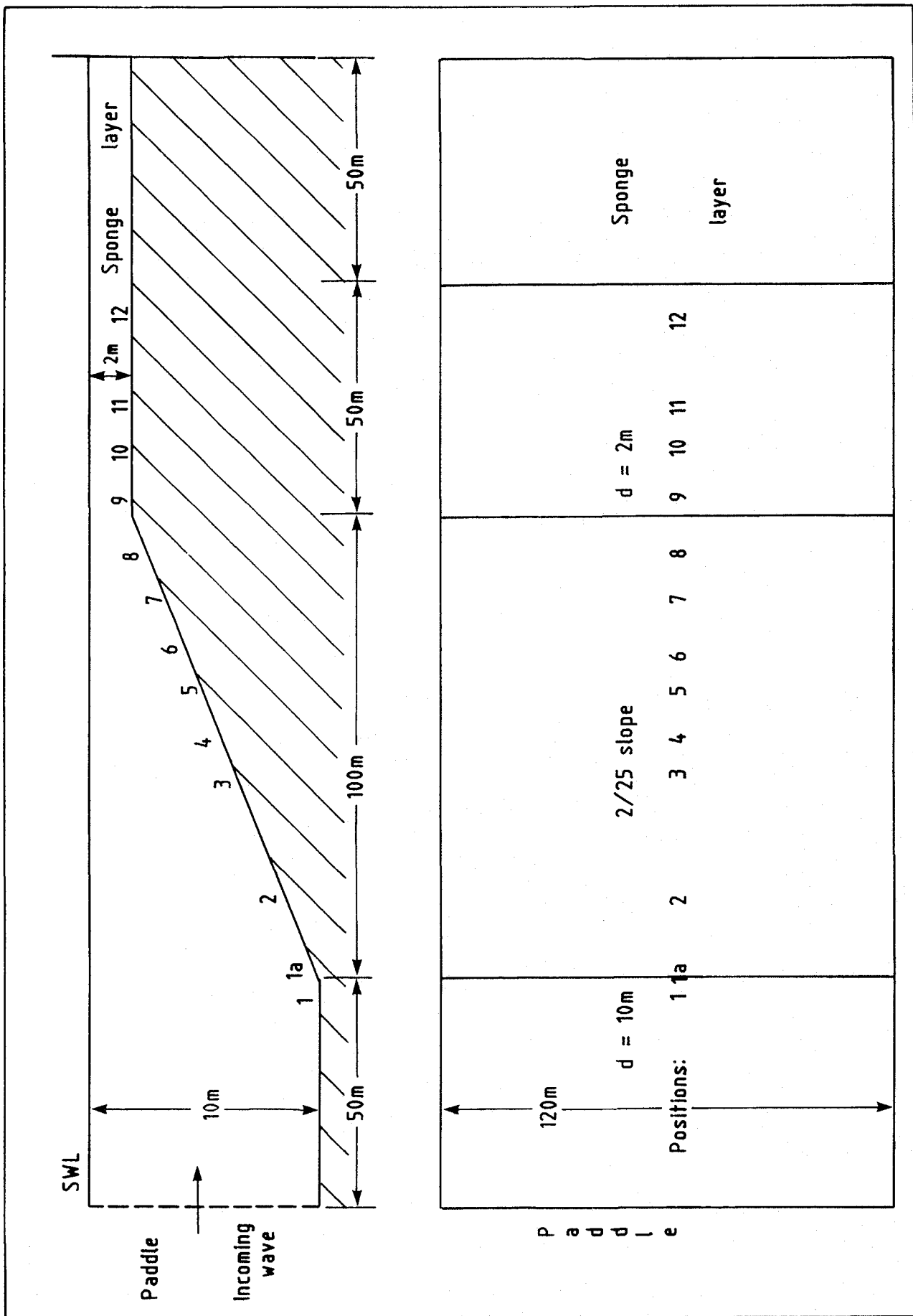


Fig 1 Profile and plan of bathymetry A : One dimensional shoal.

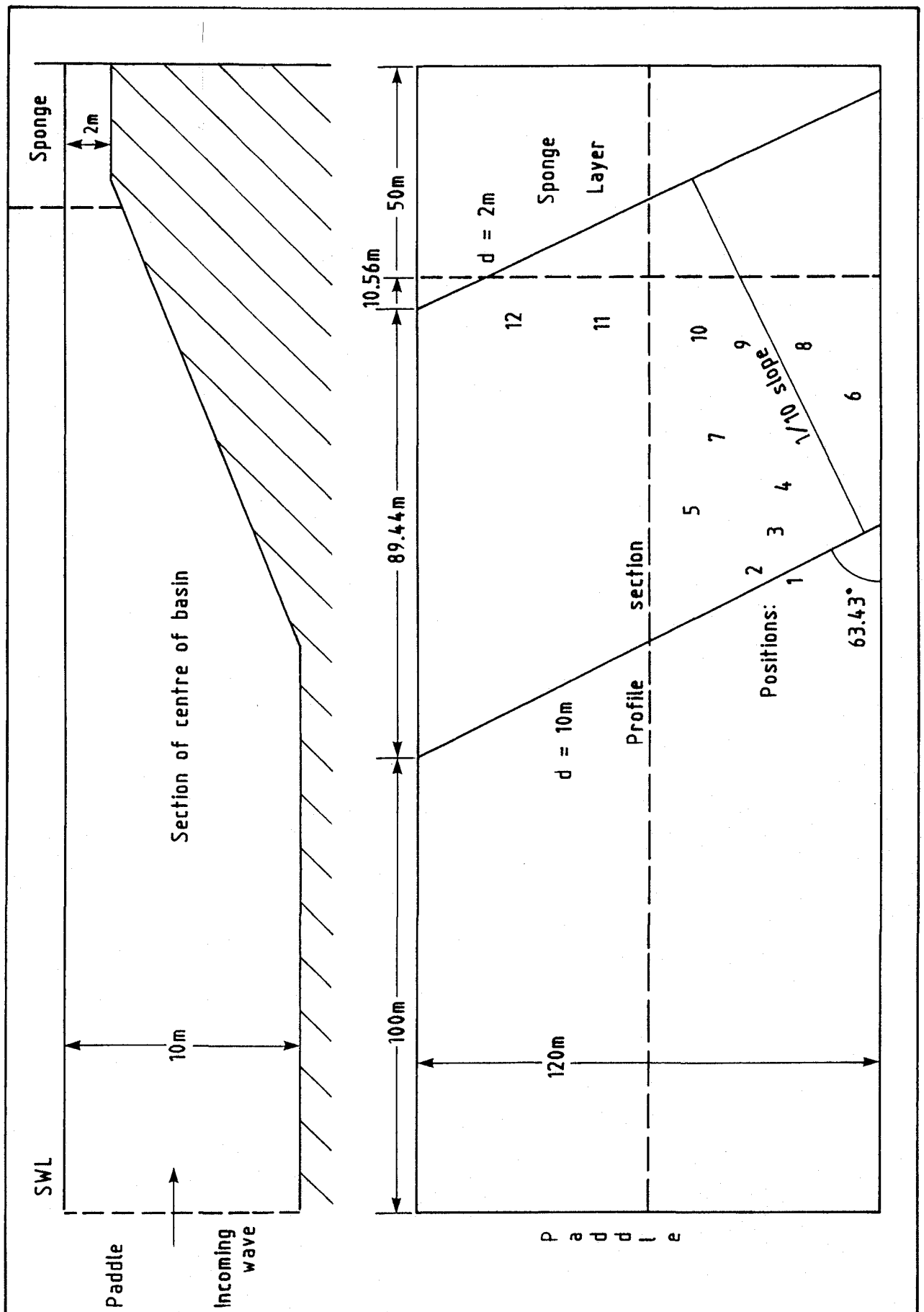


Fig 2 Profile and plan of bathymetry B : Shoal and refraction

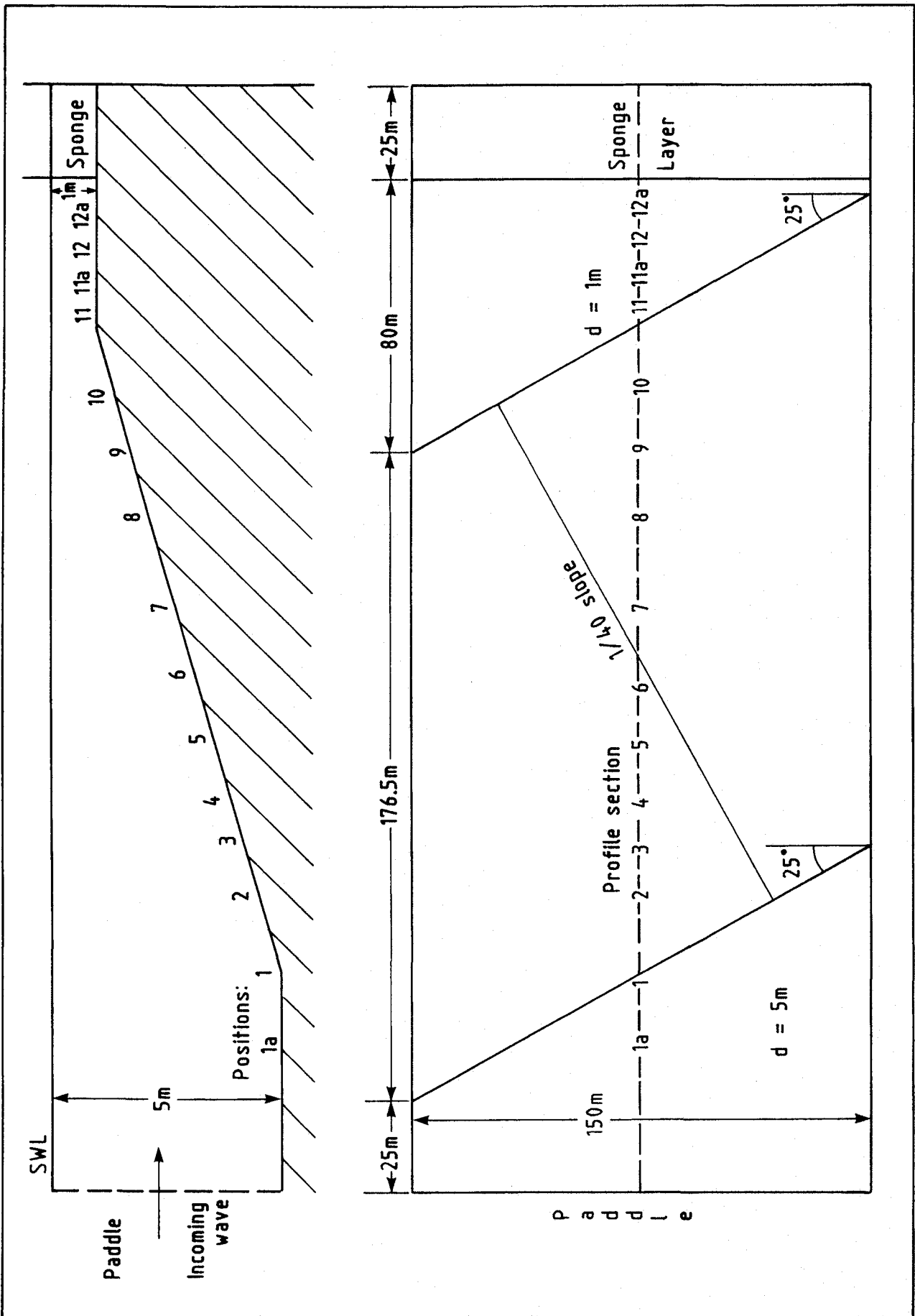


Fig 3 Profile and plan of bathymetry C : Alternative shoal and refraction

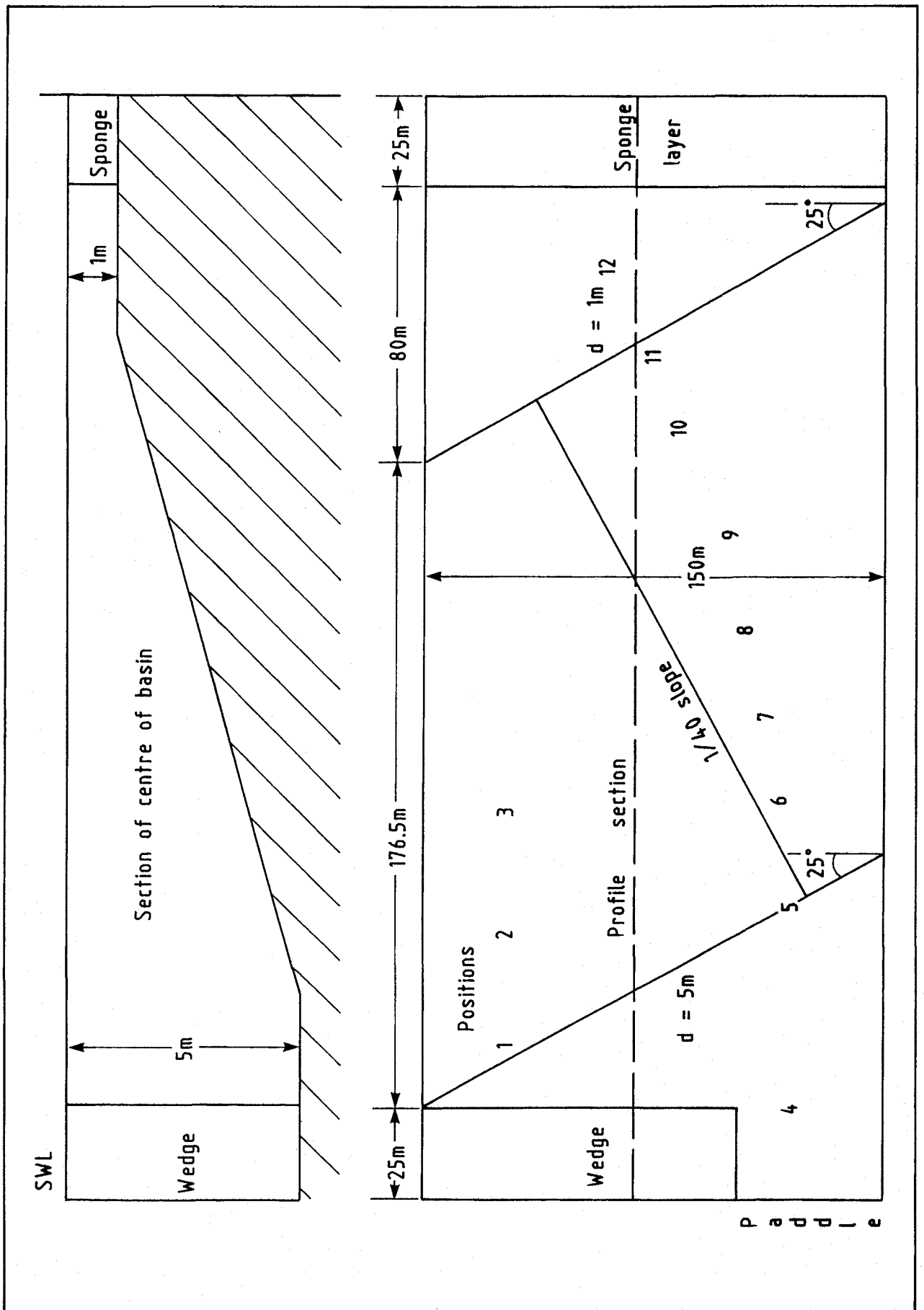


Fig 4 Profile and plan of bathymetry D : Alternative shoal and refraction with wedge breakwater

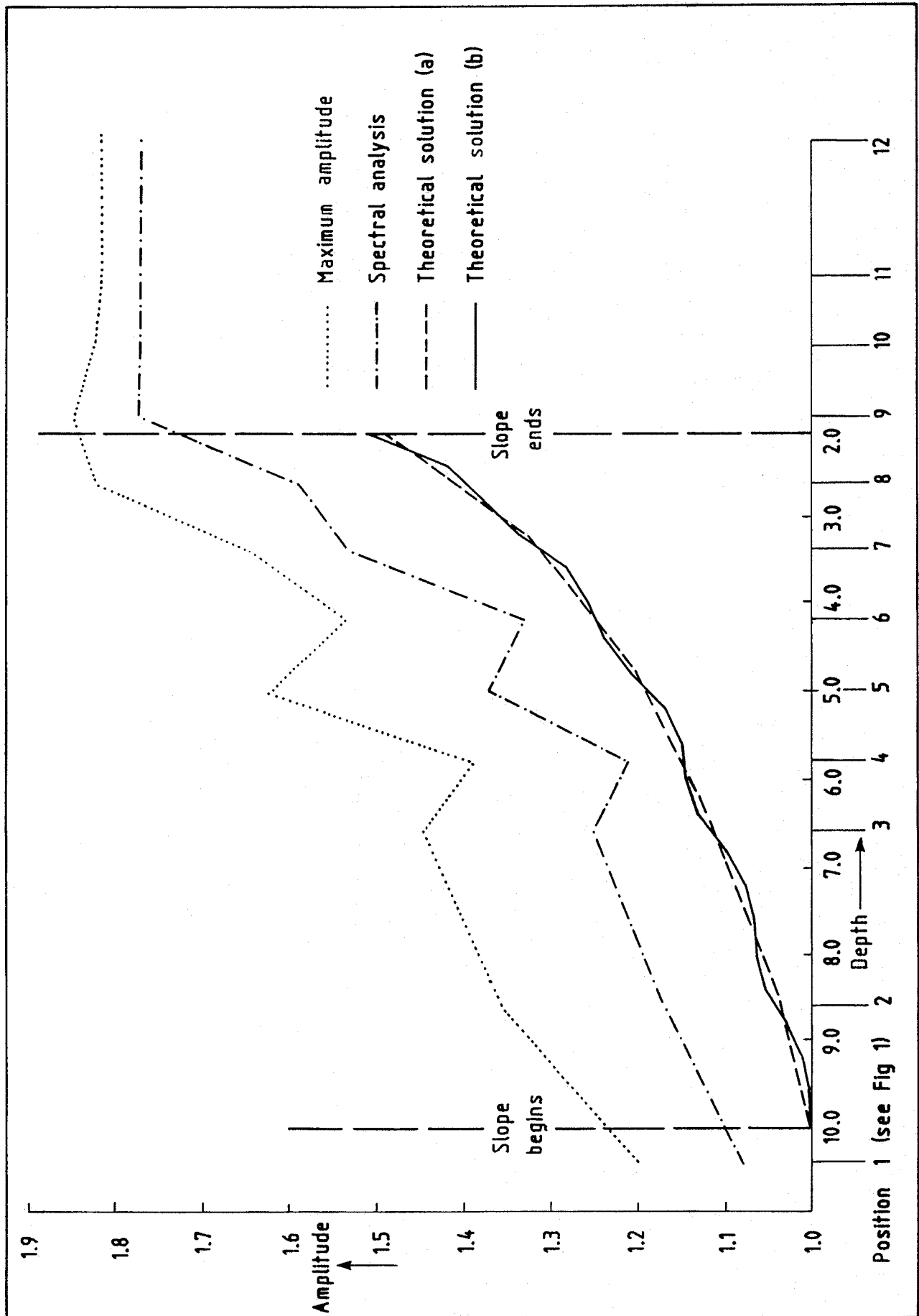


Fig 5

Numerical solution of 1D linear shallow water equations, see eqns (2.4) & (2.5), for bathymetry A, period  $T = 6s$ . Input wave amplitude = 1.0m

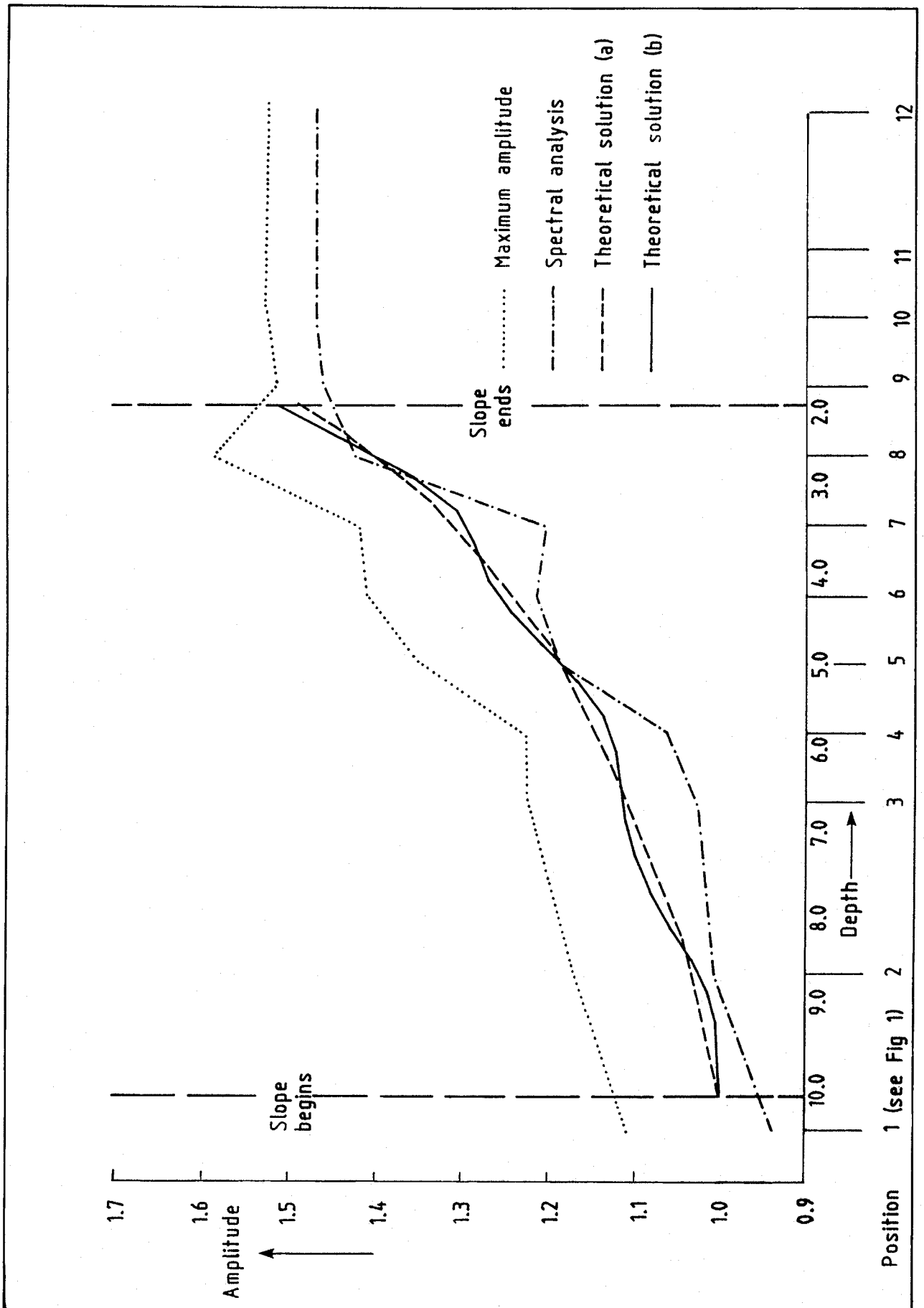


Fig 6 Numerical solution of 1D linear shallow water equations, see eqns (2.4) & (2.5), for bathymetry A, period  $T = 10s$  Input wave amplitude = 1.0m

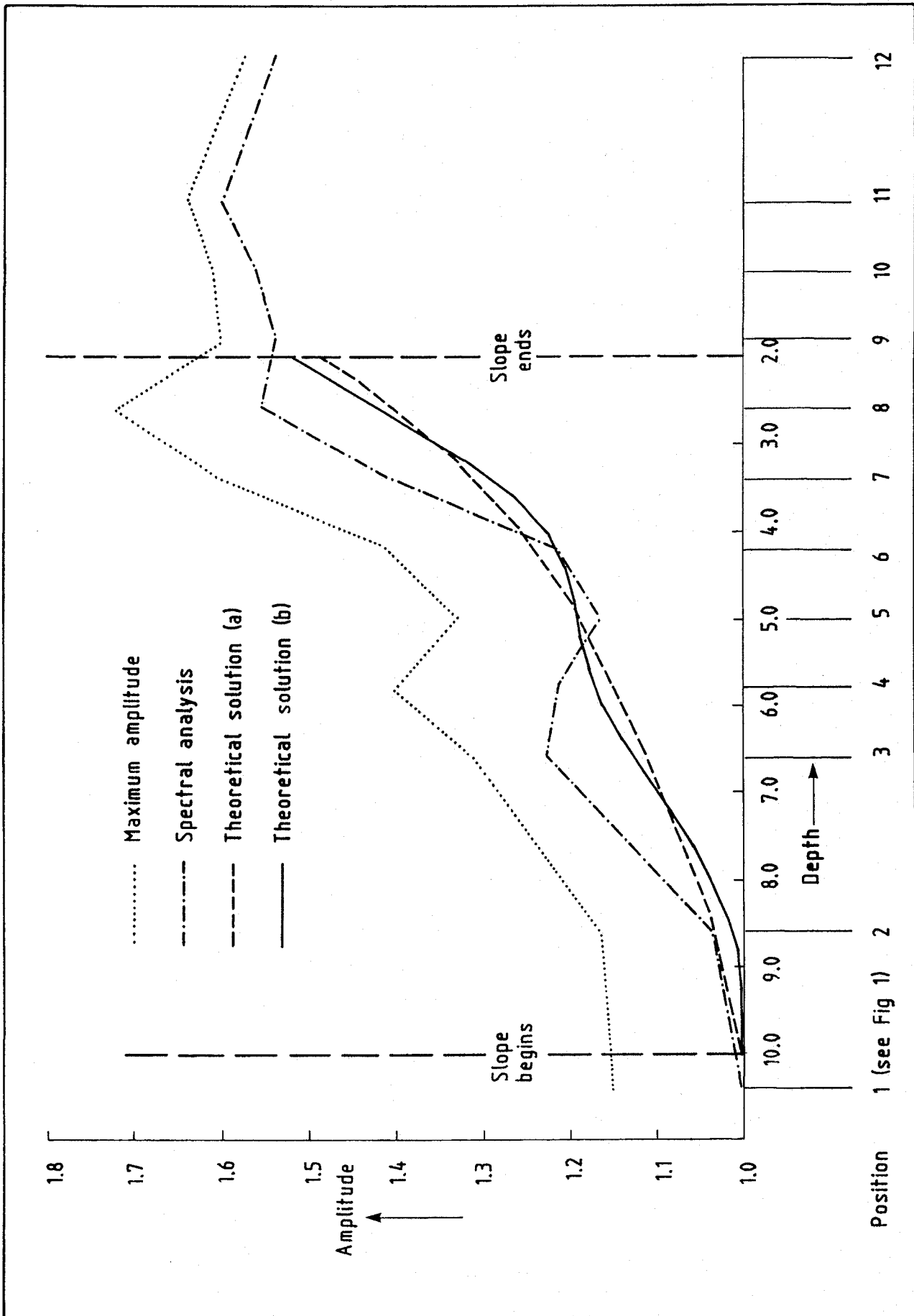


Fig 7 Numerical solution of 1D linear shallow water equations, see eqns (2.4) & (2.5), for bathymetry A, period  $T = 15s$ . Input wave amplitude = 1.0m

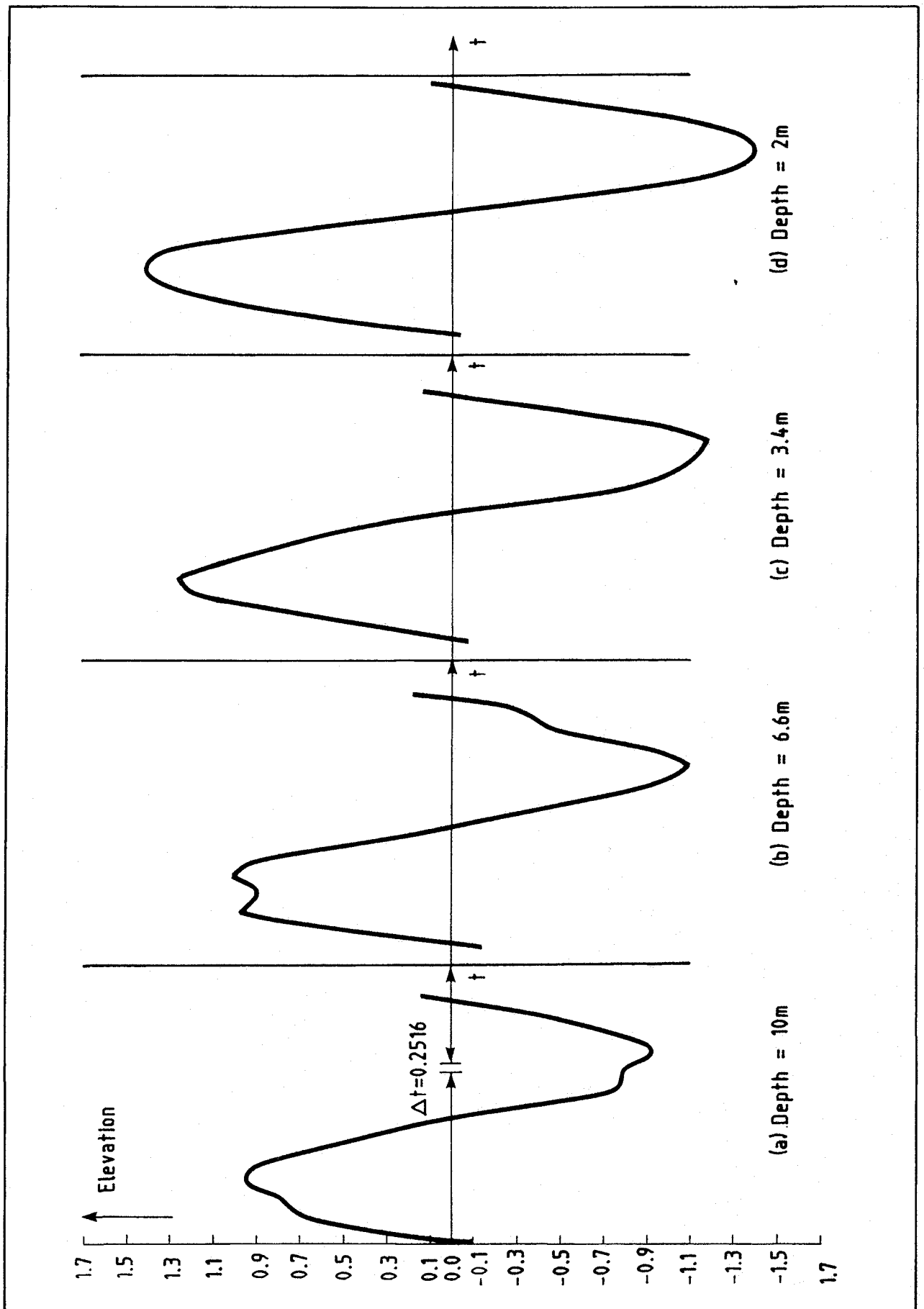


Fig 8 Wave elevation plotted against time at four surface points, period  $T = 10\text{s}$ , with bathymetry A. Numerical solution of equations (2.4) & (2.5). Input wave amplitude = 1.0m.

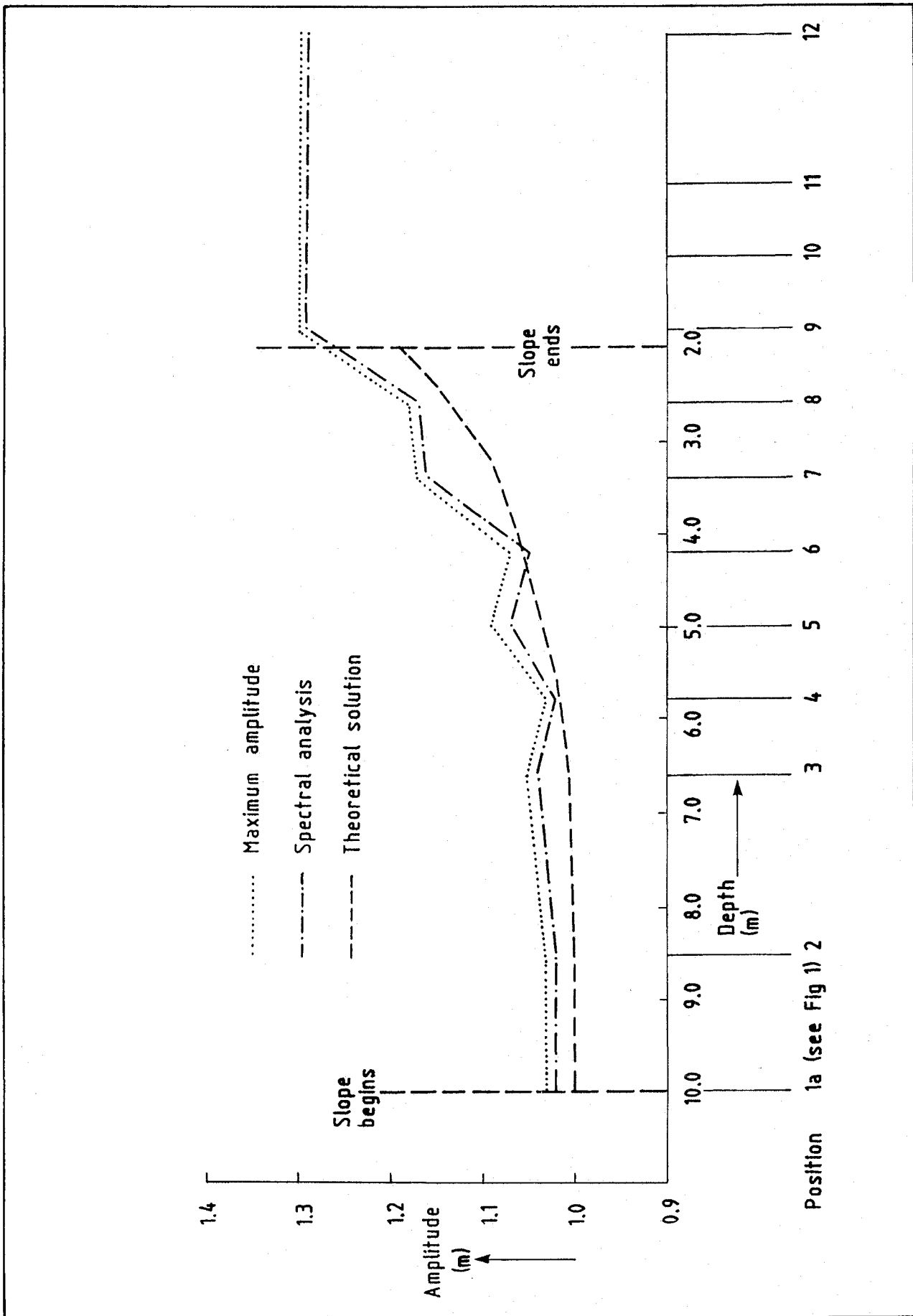


Fig 9 Numerical results showing the effect of introducing dispersion. Solution of equations (2.6) & (2.7), bathymetry A,  $T = 6s$ . Input wave amplitude = 1.0m

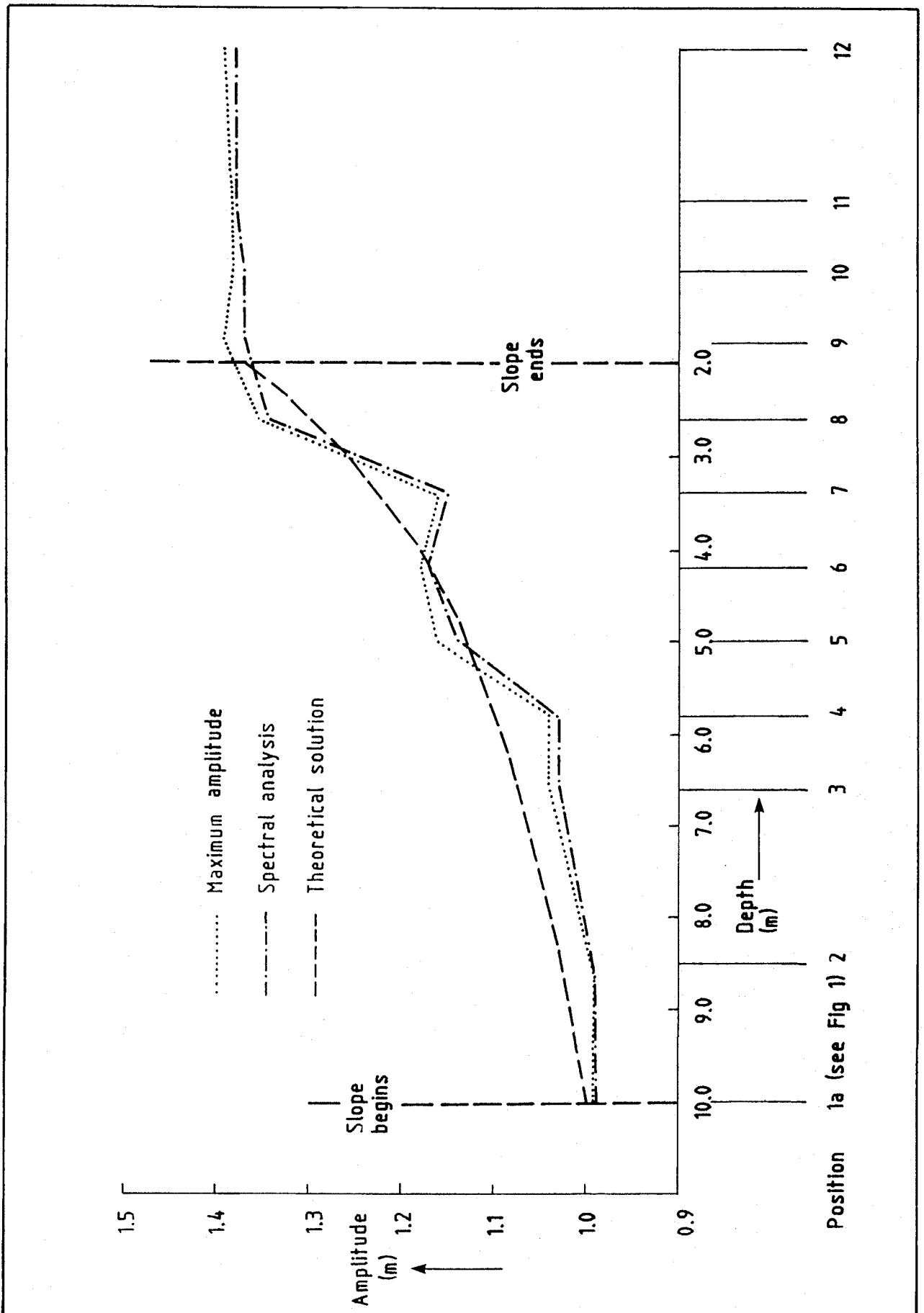


Fig 10

Numerical results showing the effect of introducing dispersion. Solution of equations (2.6) & (2.7), bathymetry A,  $T = 10s$ . Input wave amplitude = 1.0m

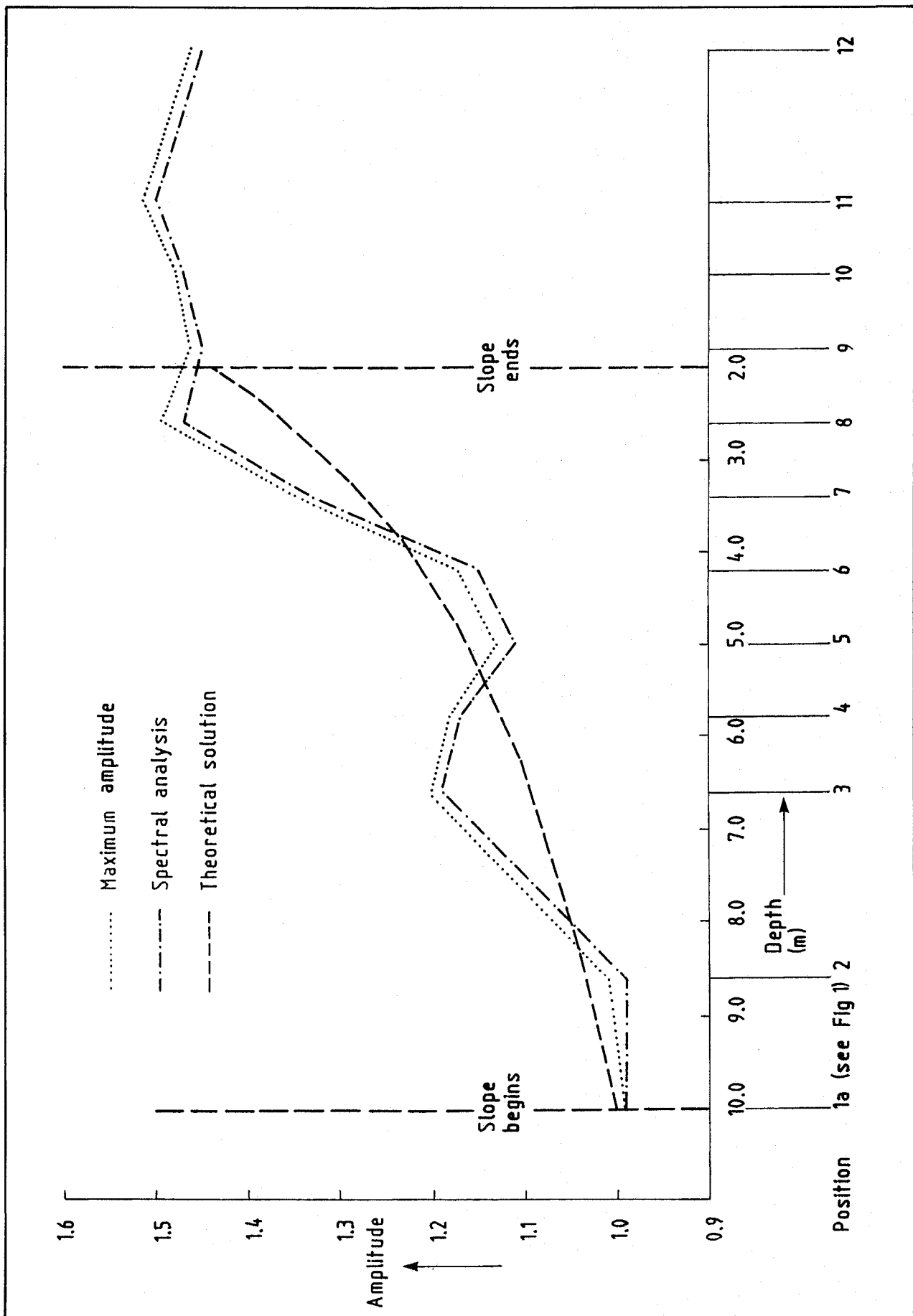


Fig 11 Numerical results showing the effect of introducing dispersion. Solution of equations (2.6) & (2.7), bathymetry A,  $T = 15s$ . Input wave amplitude = 1.0m

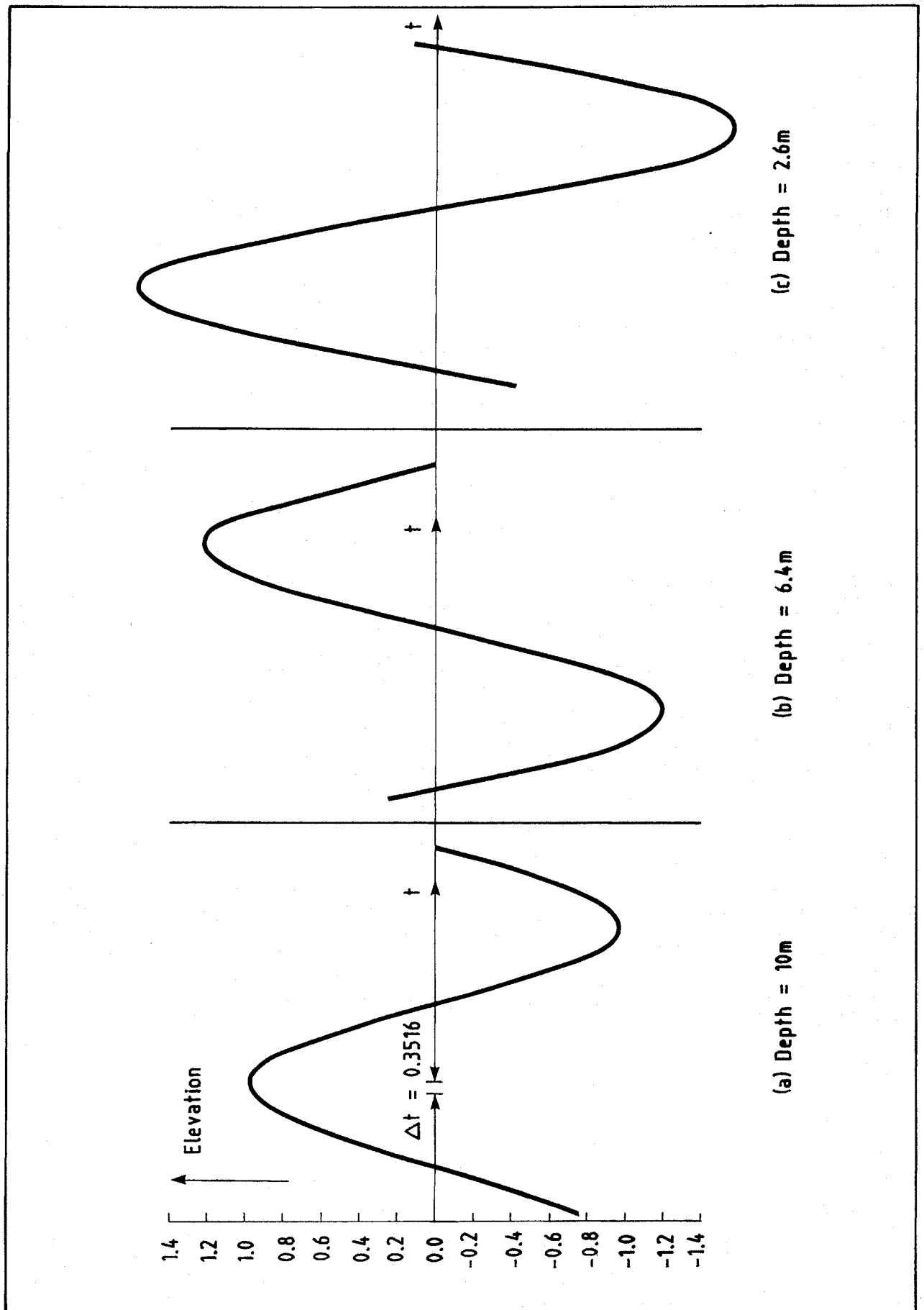


Fig 12 Wave elevation plotted against time at three surface points, period  $T = 15s$ , with bathymetry A. Numerical solution of equations (2.6) and (2.7). Input wave amplitude = 1.0m

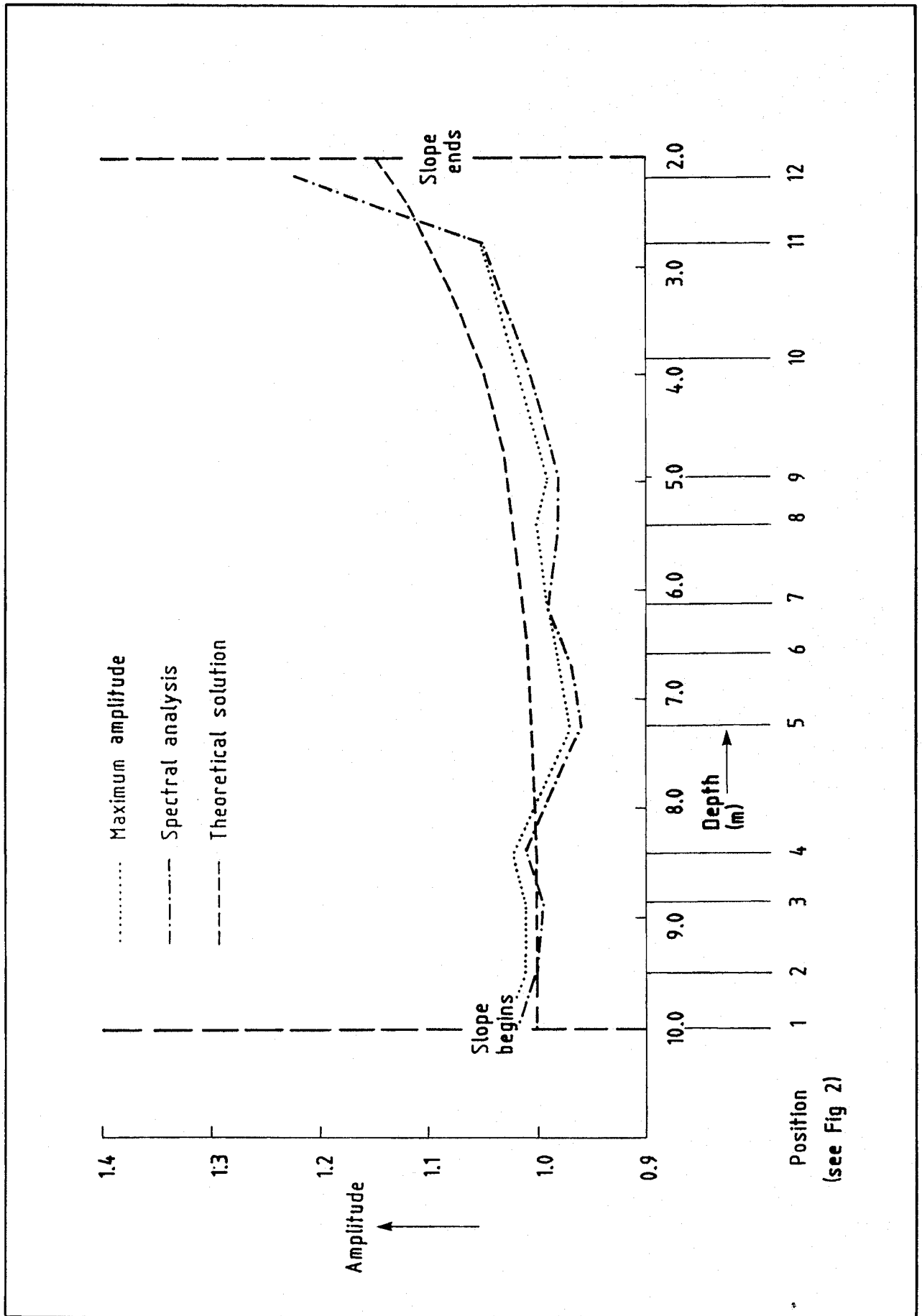


Fig 13 Numerical solution of 2 dimensional linear water equations (eqns (2.8) - (2.10) for bathymetry B, period  $T = 6s$ . Input wave amplitude = 1.0m

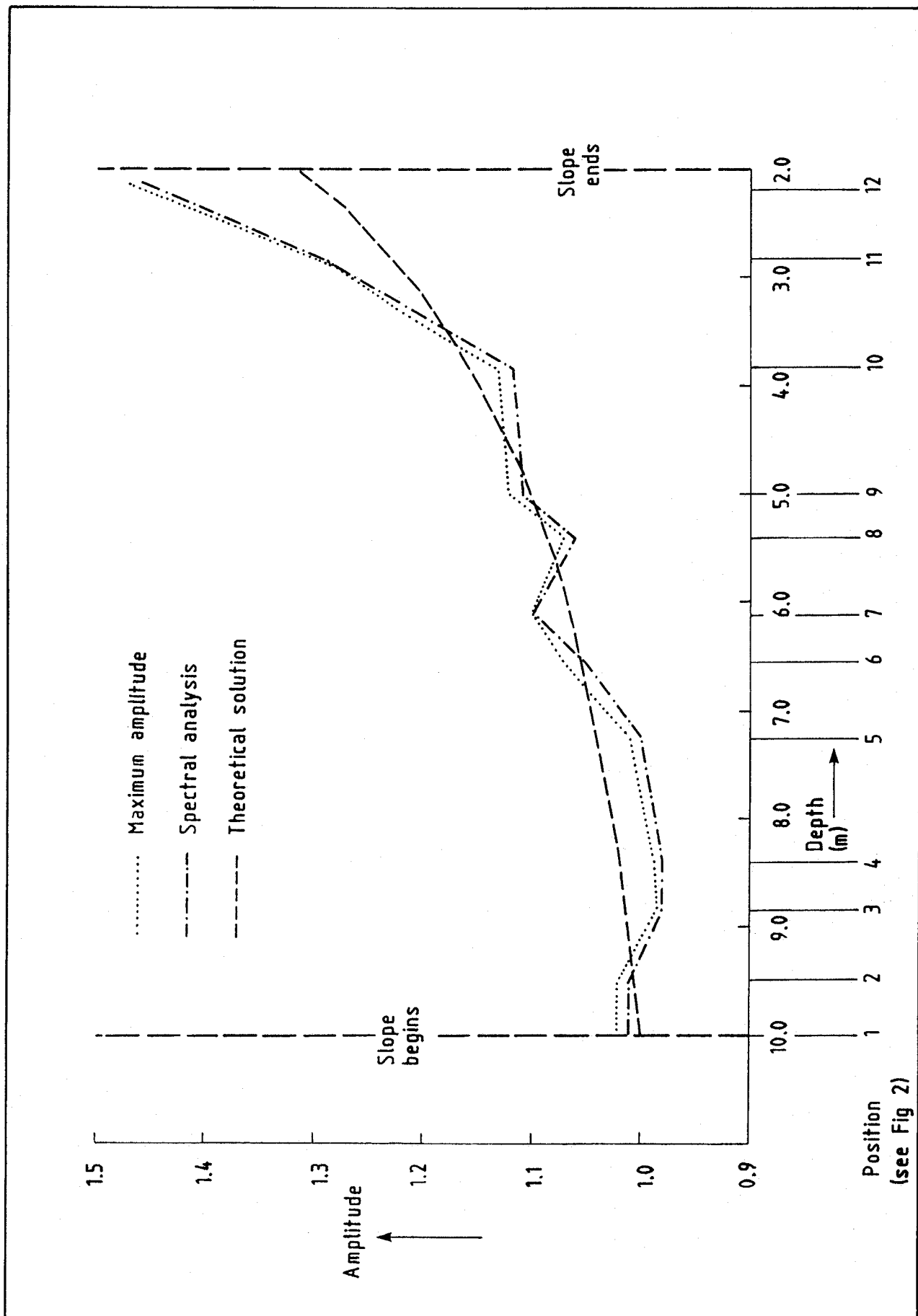


Fig 14 Numerical solution of 2 dimensional linear water equations (eqns (2.8) - (2.10)) for bathymetry B, period  $T = 10s$ . Input wave amplitude = 1.0m

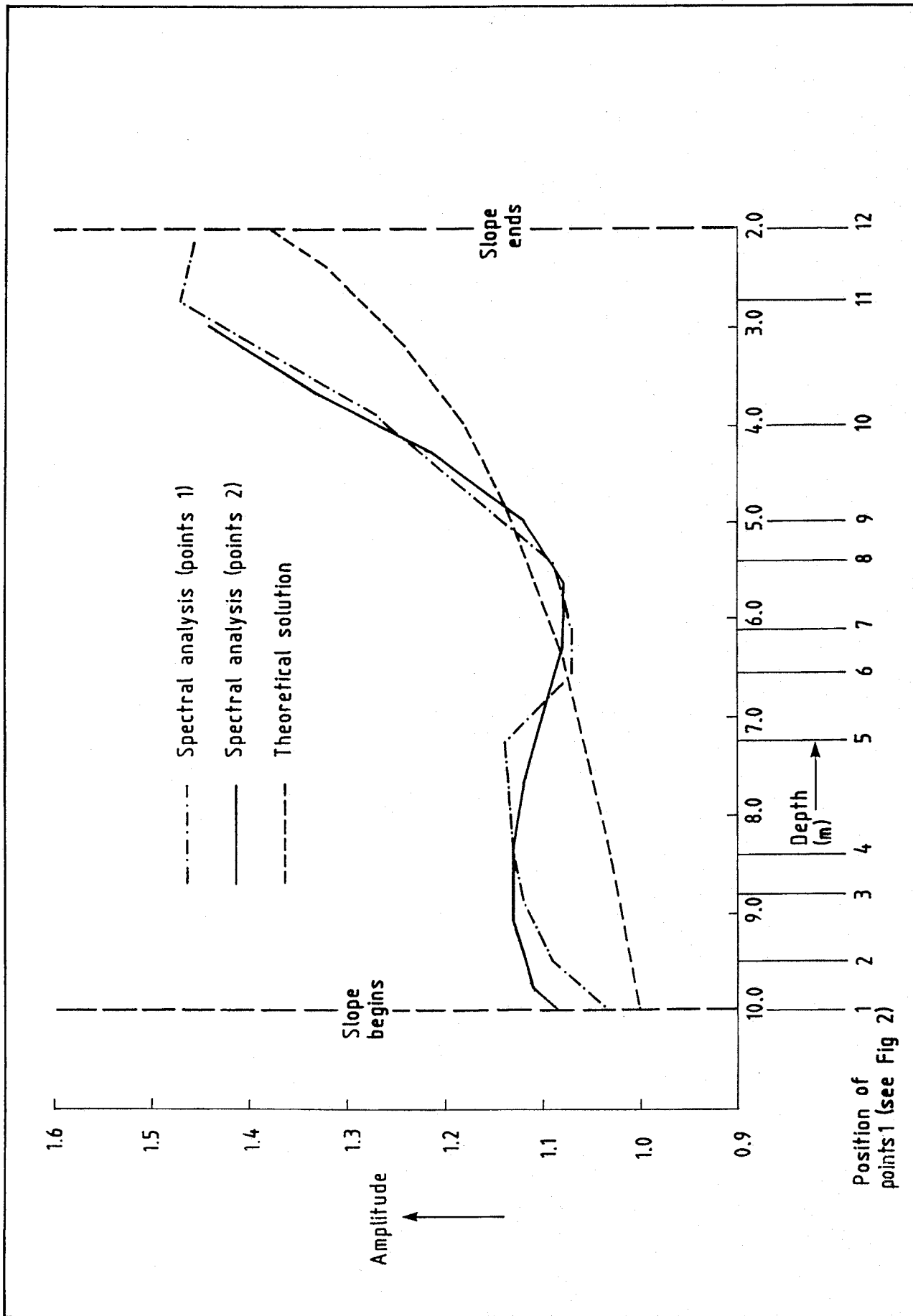


Fig 15 Numerical solution of 2 dimensional linear water equations (eqns (2.8) - (2.10)) for bathymetry B, period  $T = 15s$ . Input wave amplitude = 1.0m

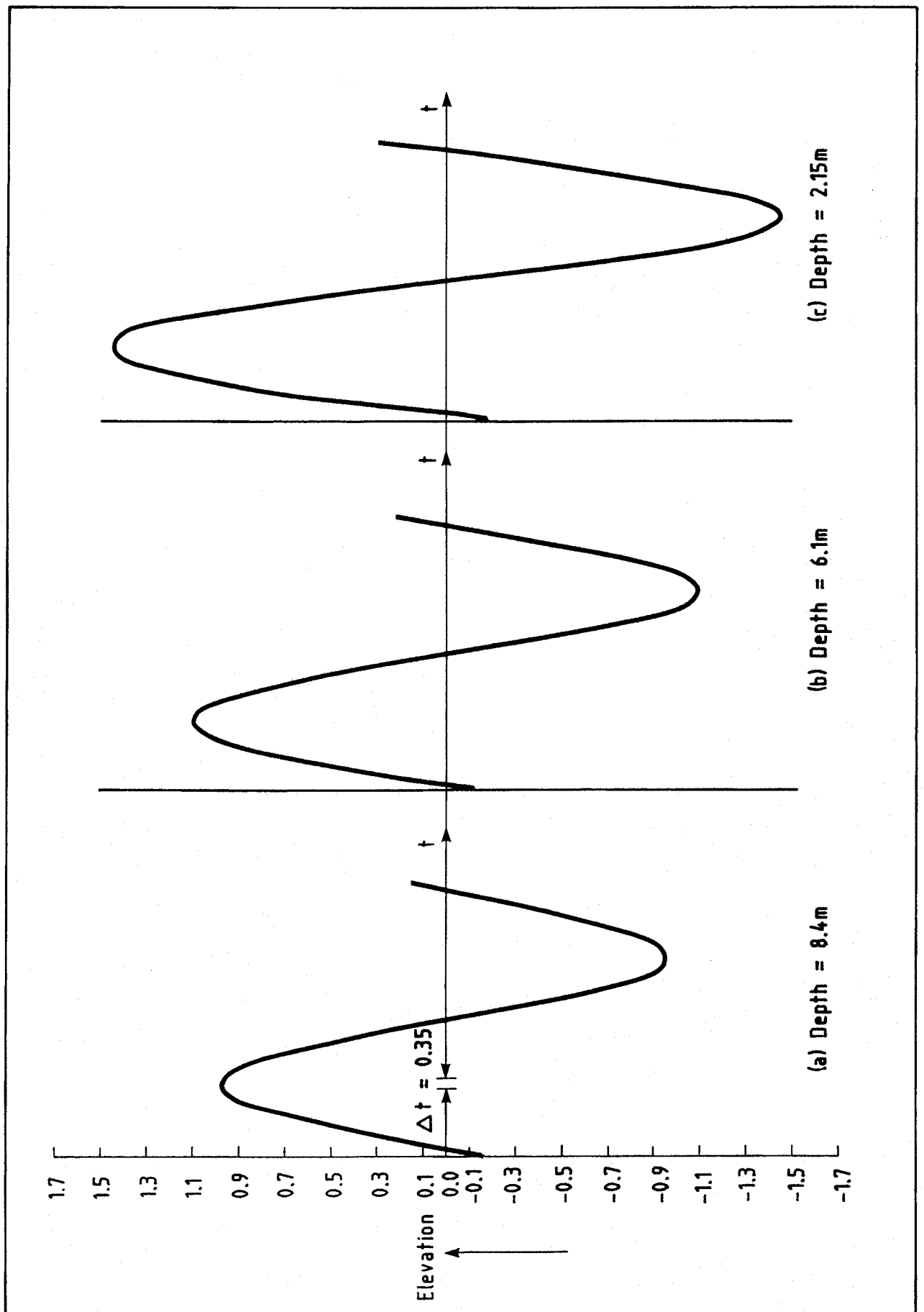


Fig 16 Wave elevation plotted against time at three surface points, period  $T = 10s$ , bathymetry B. Numerical solution of equations (2.8) - (2.10) Input wave amplitude = 1.0m

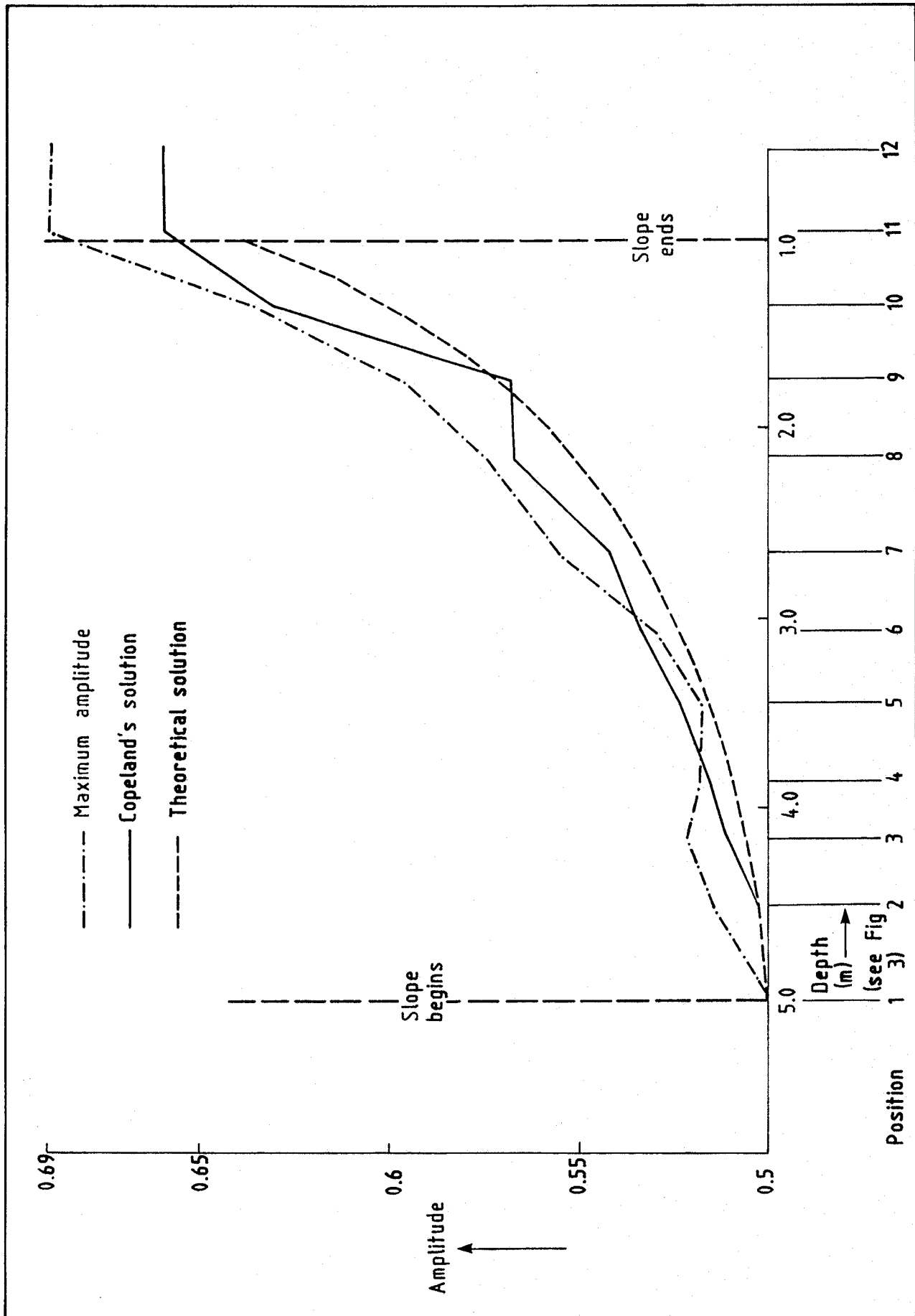


Fig 17 Numerical solution of linearised water equations (eqn (2.8) - (2.10), with bathymetry C, period  $T = 6s$ , and comparison with results of a different numerical model. Input wave amplitude = 0.5m

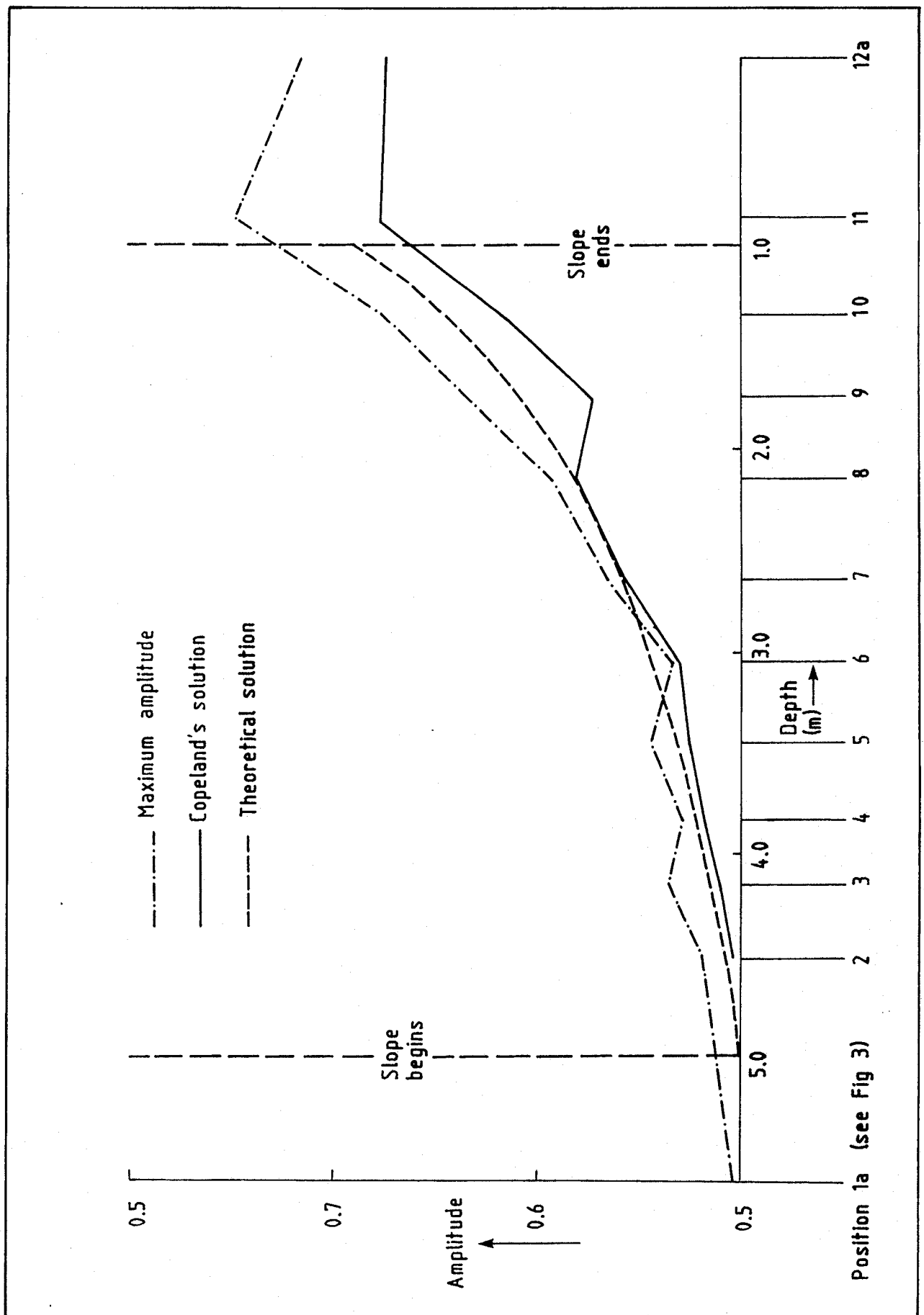


Fig 18 Numerical solution of linearised water equations (eqns.(2.8) - (2.10), with bathymetry C, period  $T = 10s$ , and comparison with results of a different numerical model. Input wave amplitude = 0.5m

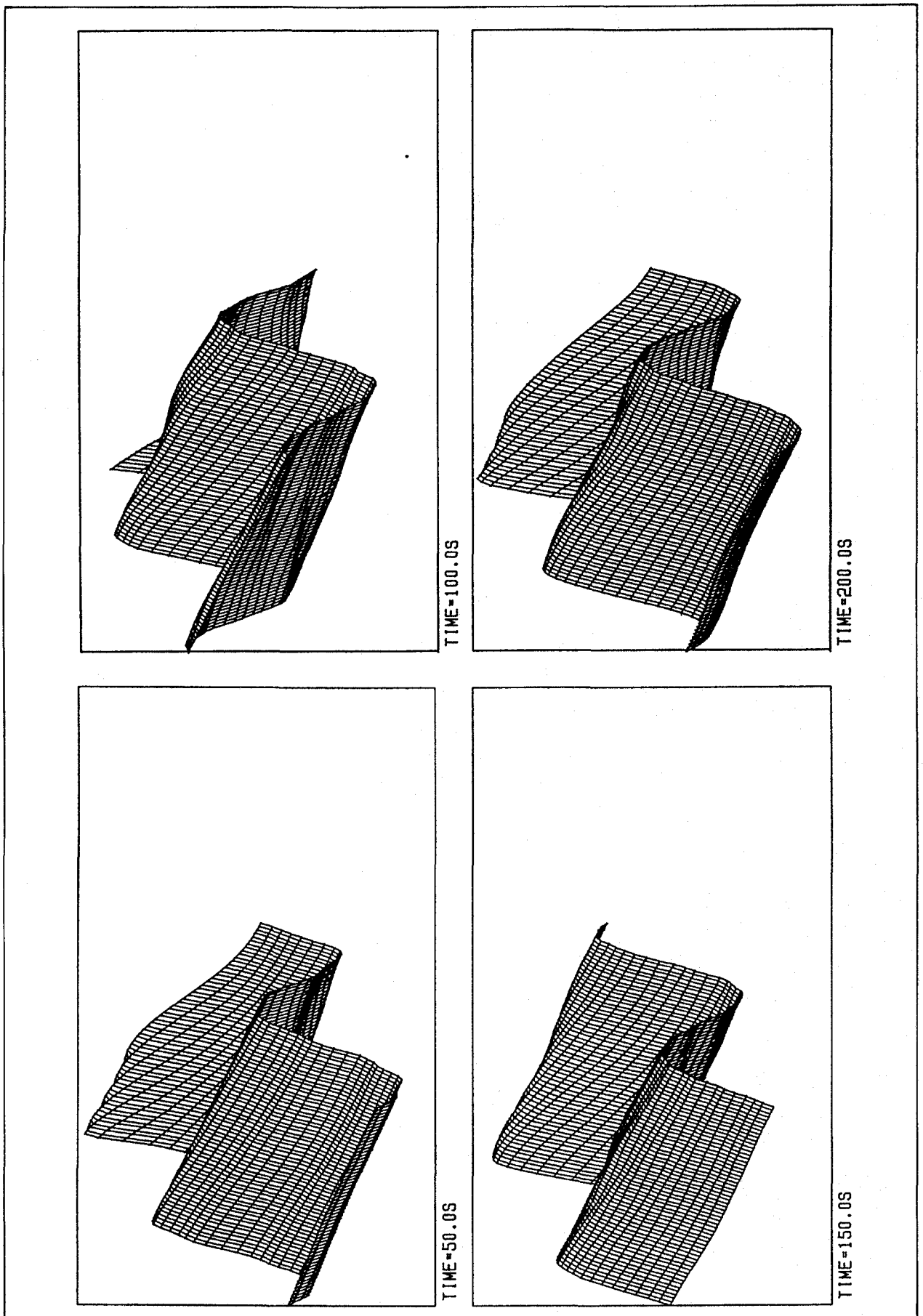


Fig 19 Surface wave elevation across part of basin with bathymetry C, for period  $T = 15s$ , at times 50s, 100s, 150s and 200s after start. ( $\Delta t = 0.25s$ )

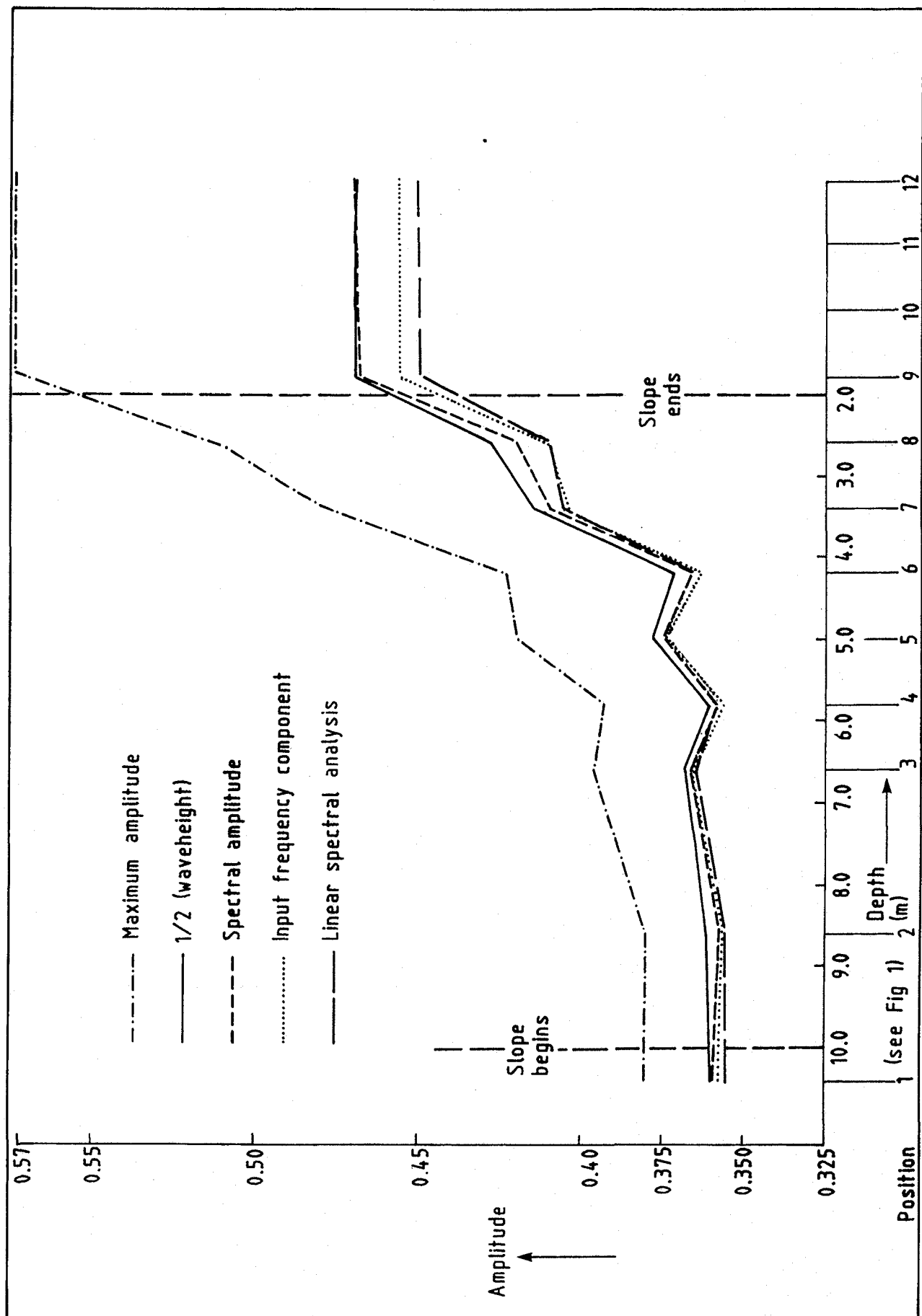


Fig 20 Numerical solution of non-linear water equations (see eqns (2.1)-(2.3)), with bathymetry A, period  $T = 6s$ . Input wave amplitude = 0.35m

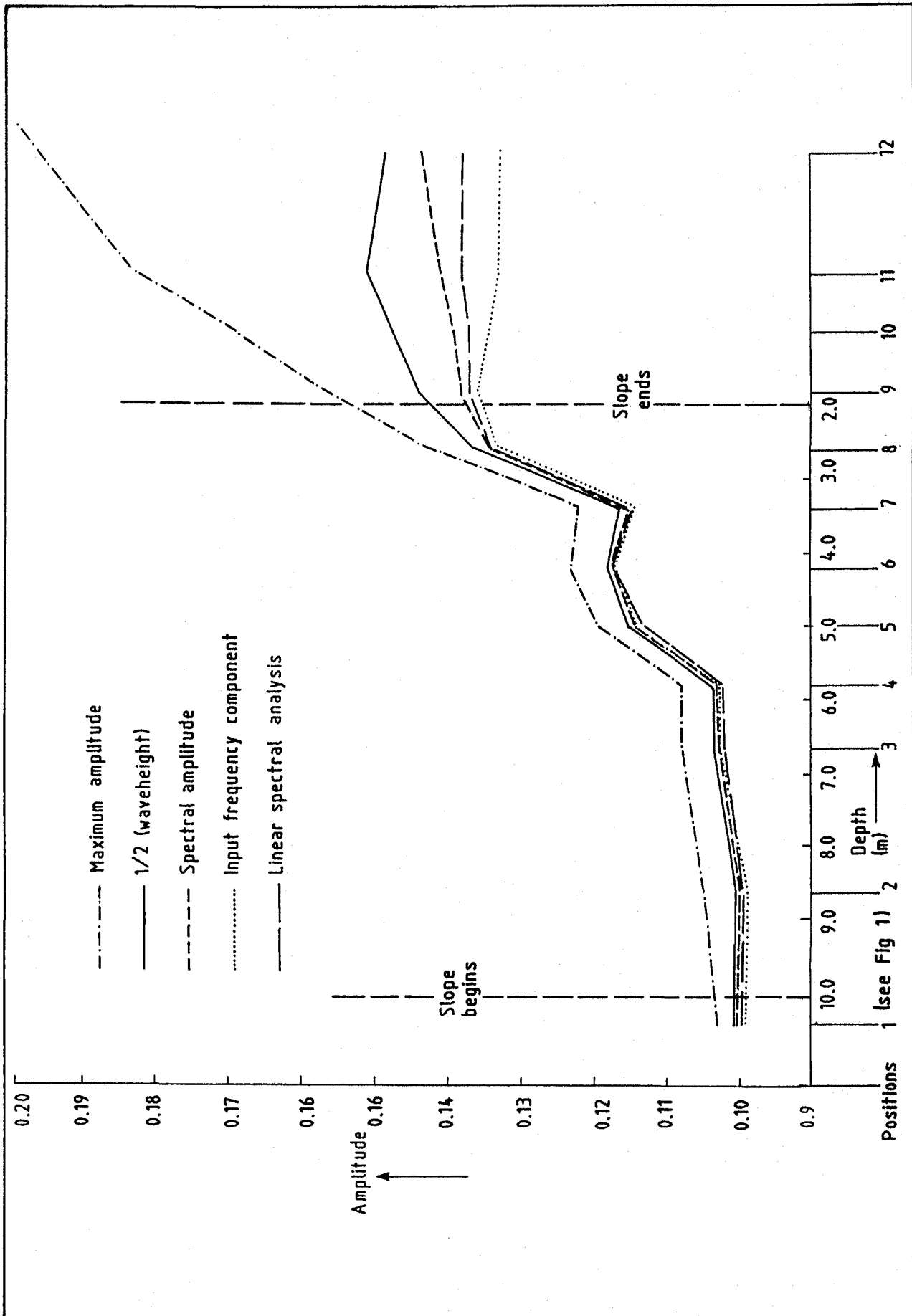


Fig 21 Numerical solution of non-linear water equations (see eqns (2.1) - (2.3)), with bathymetry A, period  $T = 10s$ . Input wave amplitude =  $0.1m$

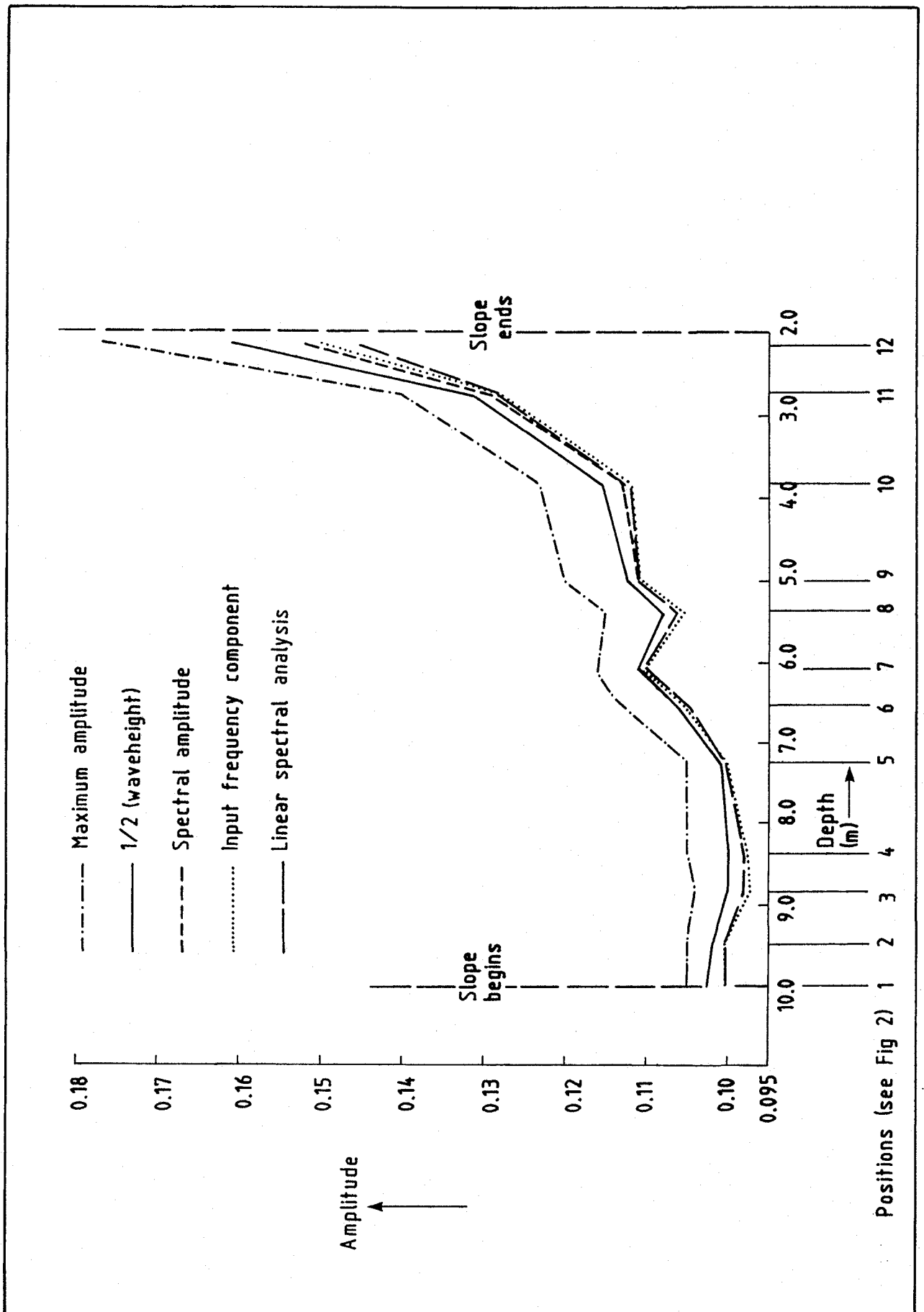


Fig 22 Numerical solution of non-linear water equations (see eqns (2.1) - (2.3)), with bathymetry B, period  $T = 10$ s. Input wave amplitude = 0.1m

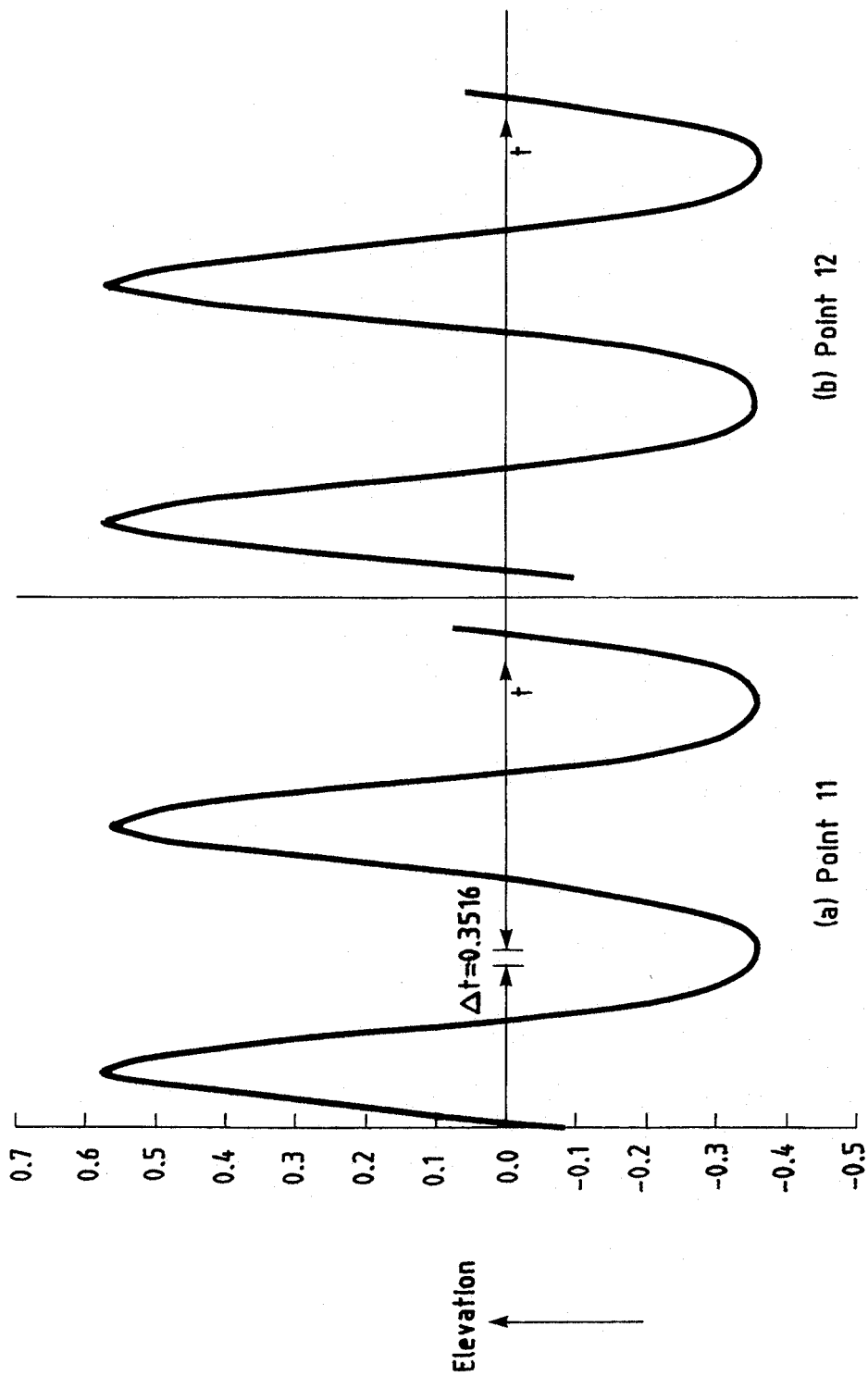


Fig 23 Wave elevation plotted against time at points 11 and 12, bathymetry A (see Fig 1), non-linear solution, period  $T = 6s$ . Input wave amplitude = 0.35m

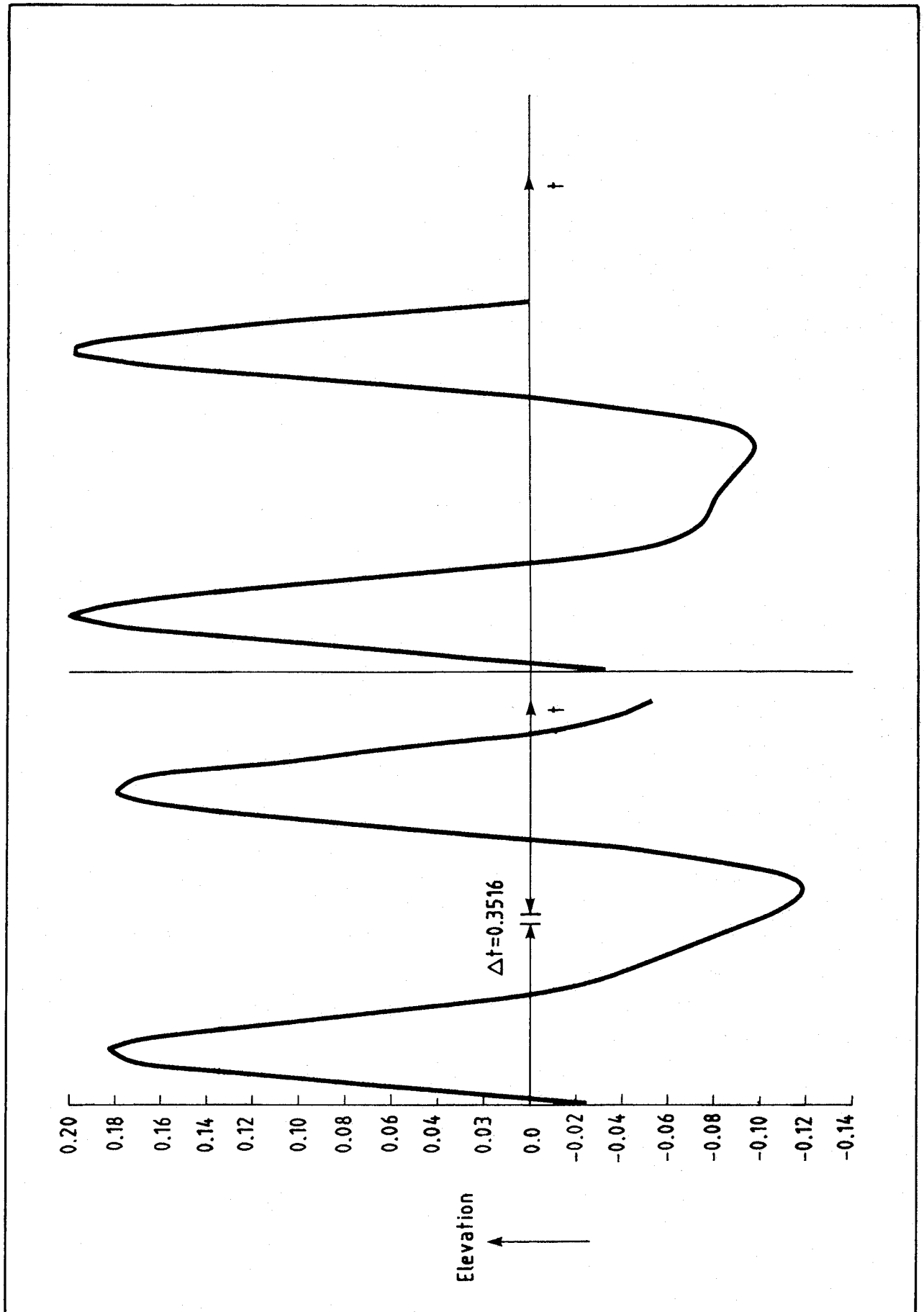
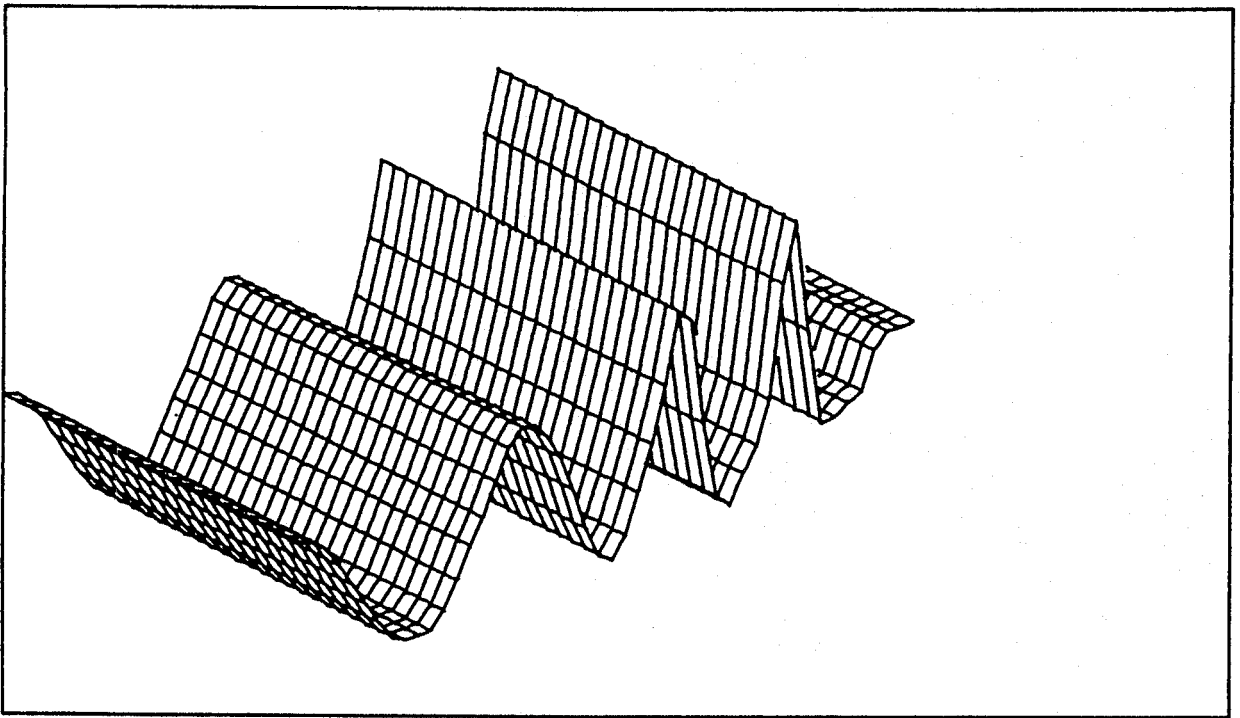
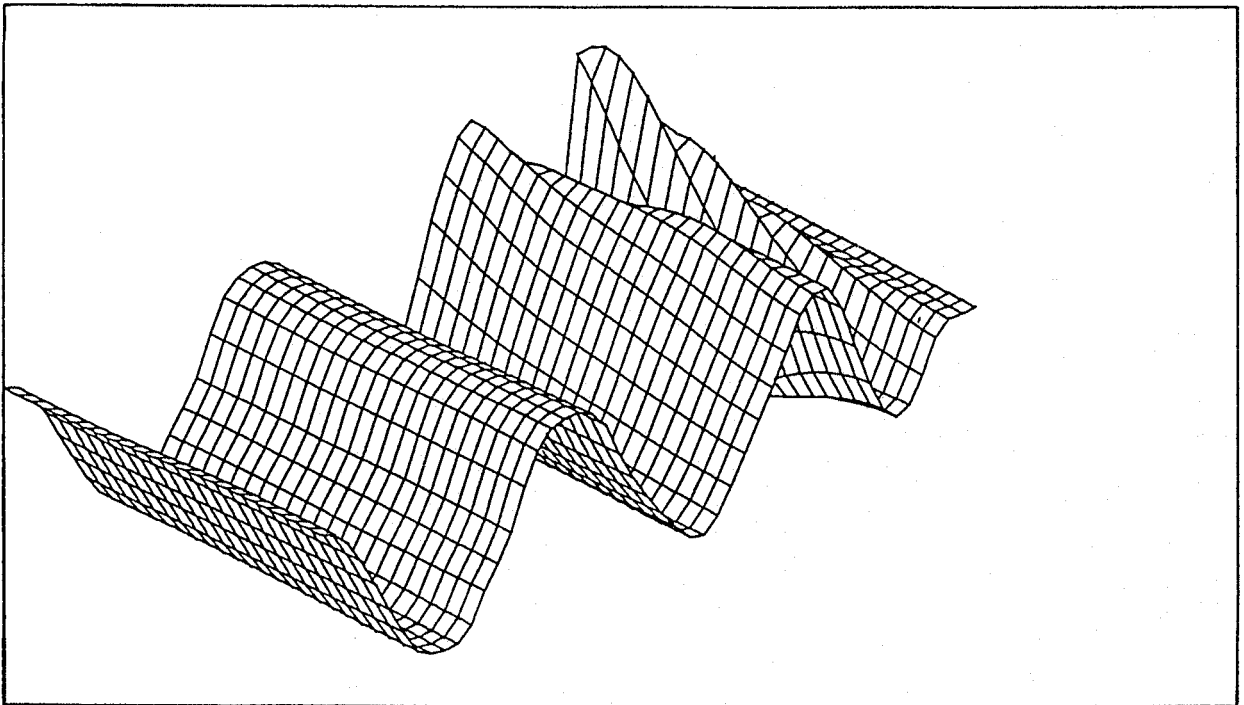


Fig 24 Wave elevation plotted against time at points 11 and 12, bathymetry A (see Fig 1), non-linear solution, period  $T = 10$ s. Input wave amplitude = 0.1m



TIME=70.32S

(a)



TIME=70.32S

(b)

Fig 25 Surface wave elevation for non-linear waves, period  $T = 10s$ , 70.32s after start, for (a) bathymetry A, (b) bathymetry B ( $\Delta t = 0.3516s$ )

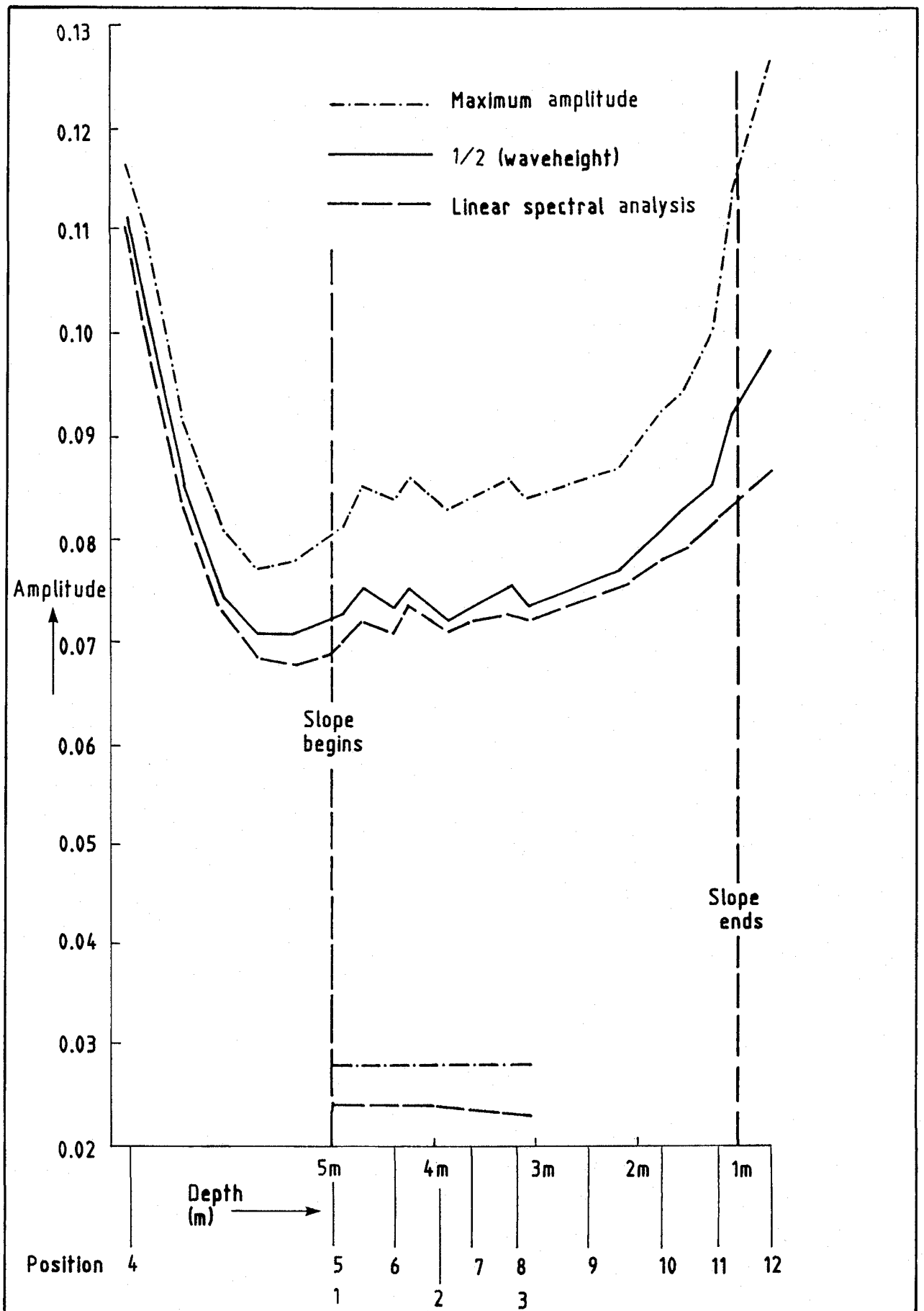


Fig 26 Linear and non-linear numerical solutions with a wedge (bathymetry D), period  $T = 10s$ . Input wave amplitude = 0.1m

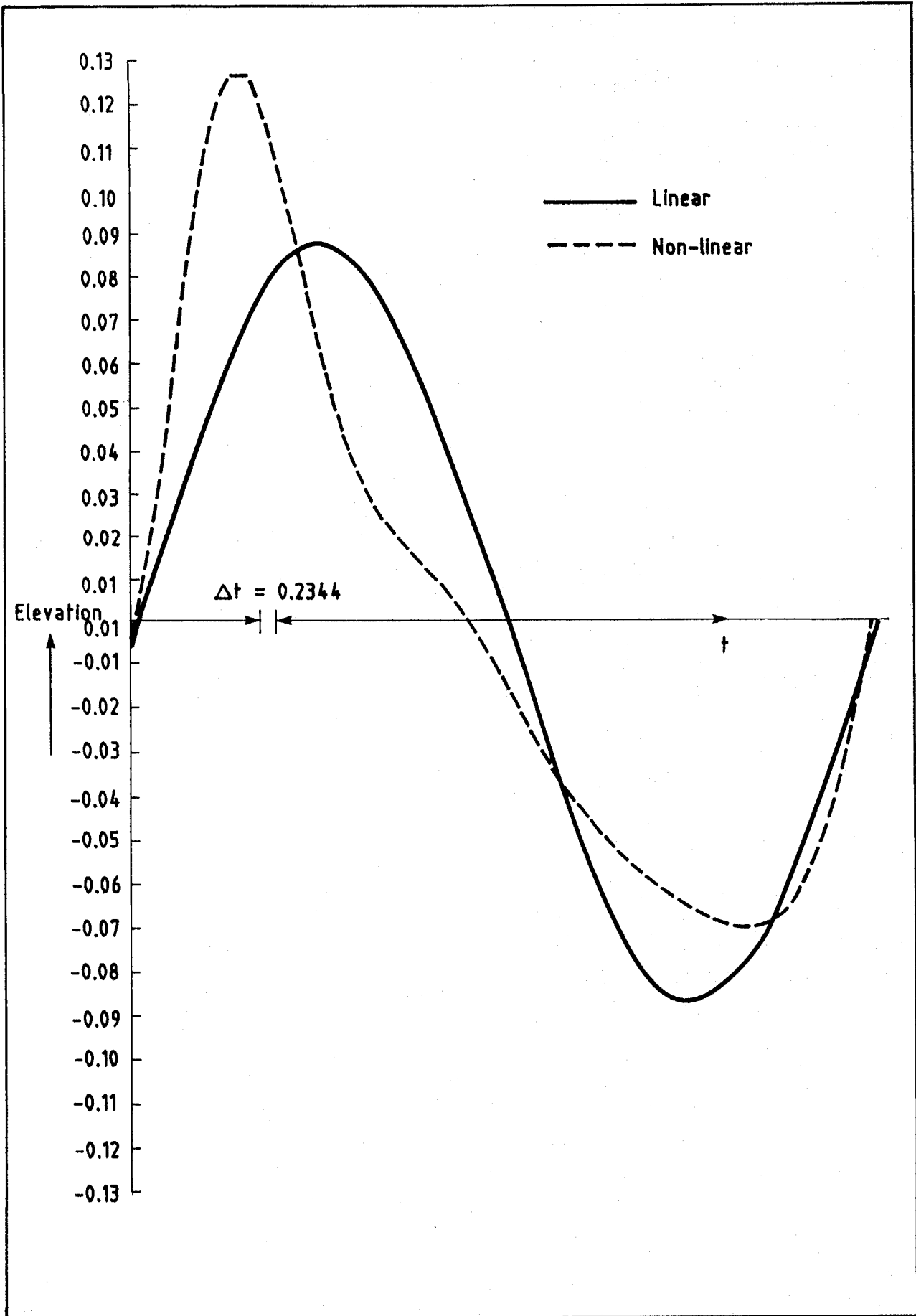


Fig 27 Wave elevation plotted against time at point 12, bathymetry D, period  $T = 10s$ , comparing the linear and non-linear solutions. Input wave amplitude = 0.1m

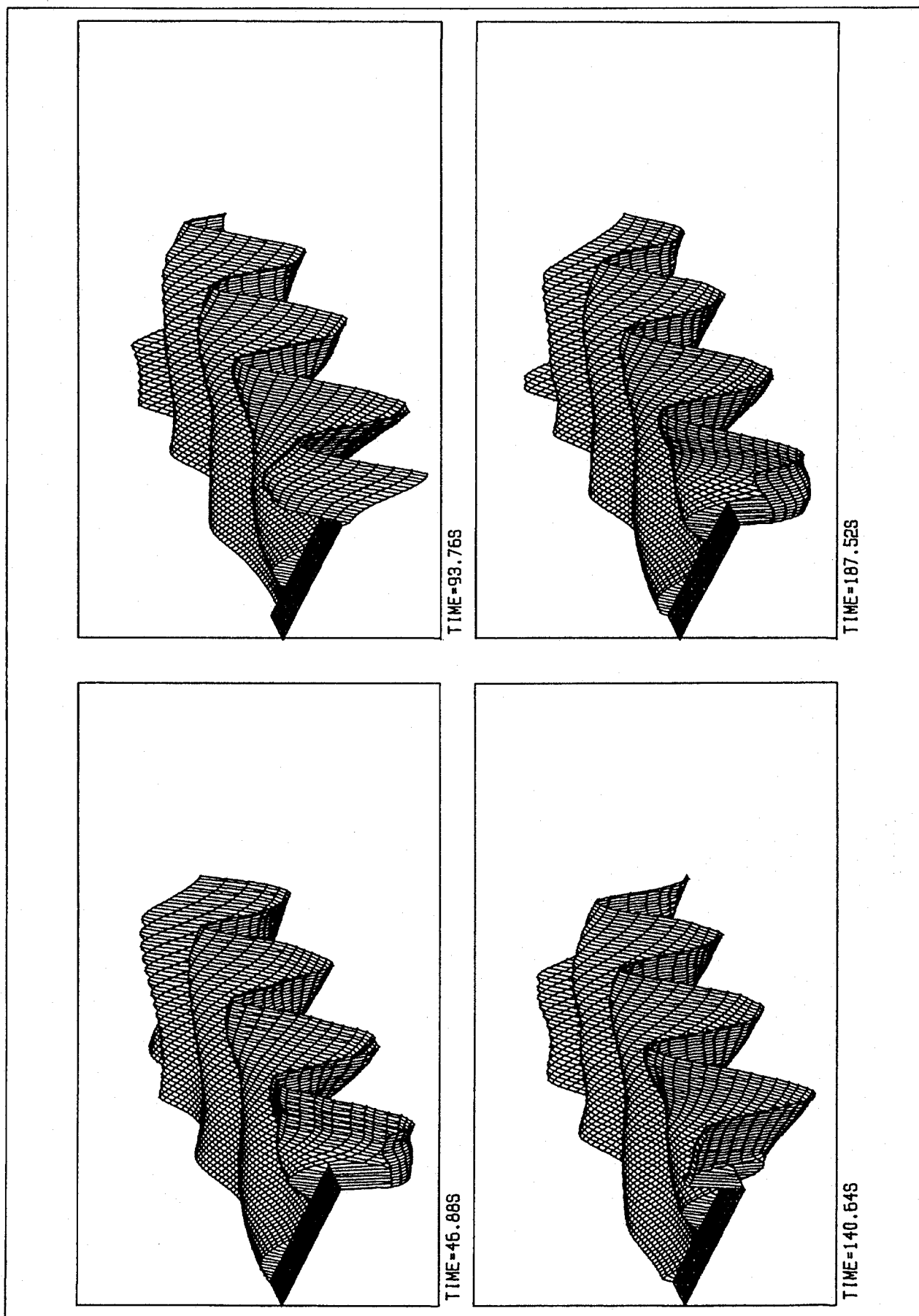


Fig 28 Surface wave elevation across part of basin with bathymetry D, for non-linear waves. Period  $T = 10s$ , elevation shown at times 46.88s, 93.76s, 140.64s and 187.52s after start. ( $\Delta t = 0.2344s$ )

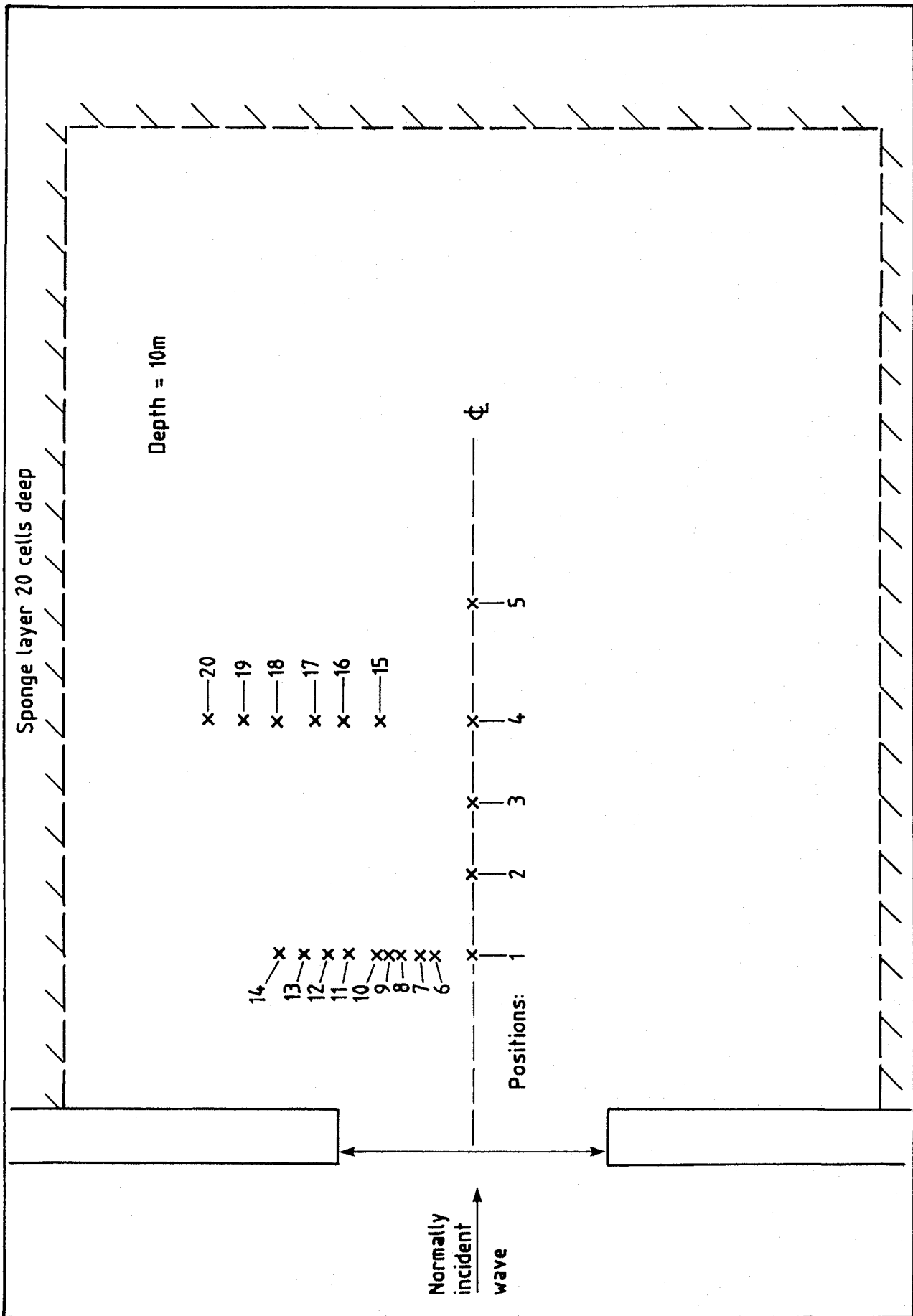


Fig 29 Breakwater gap configuration, for 10s period incident wave. Gap width =  $1.75 \times$  (wavelength)

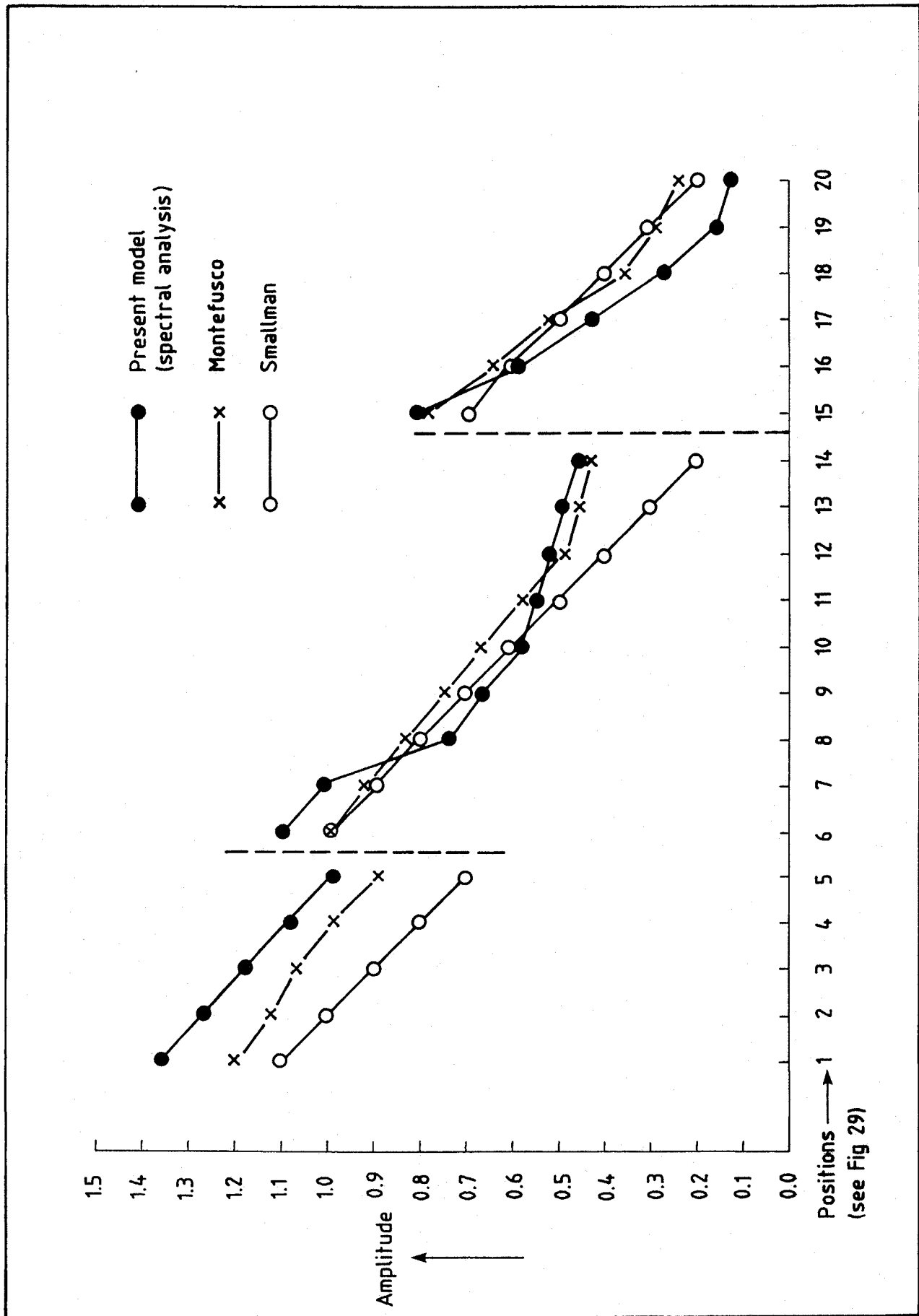


Fig 30 Diffraction by a breakwater gap, with constant water depth

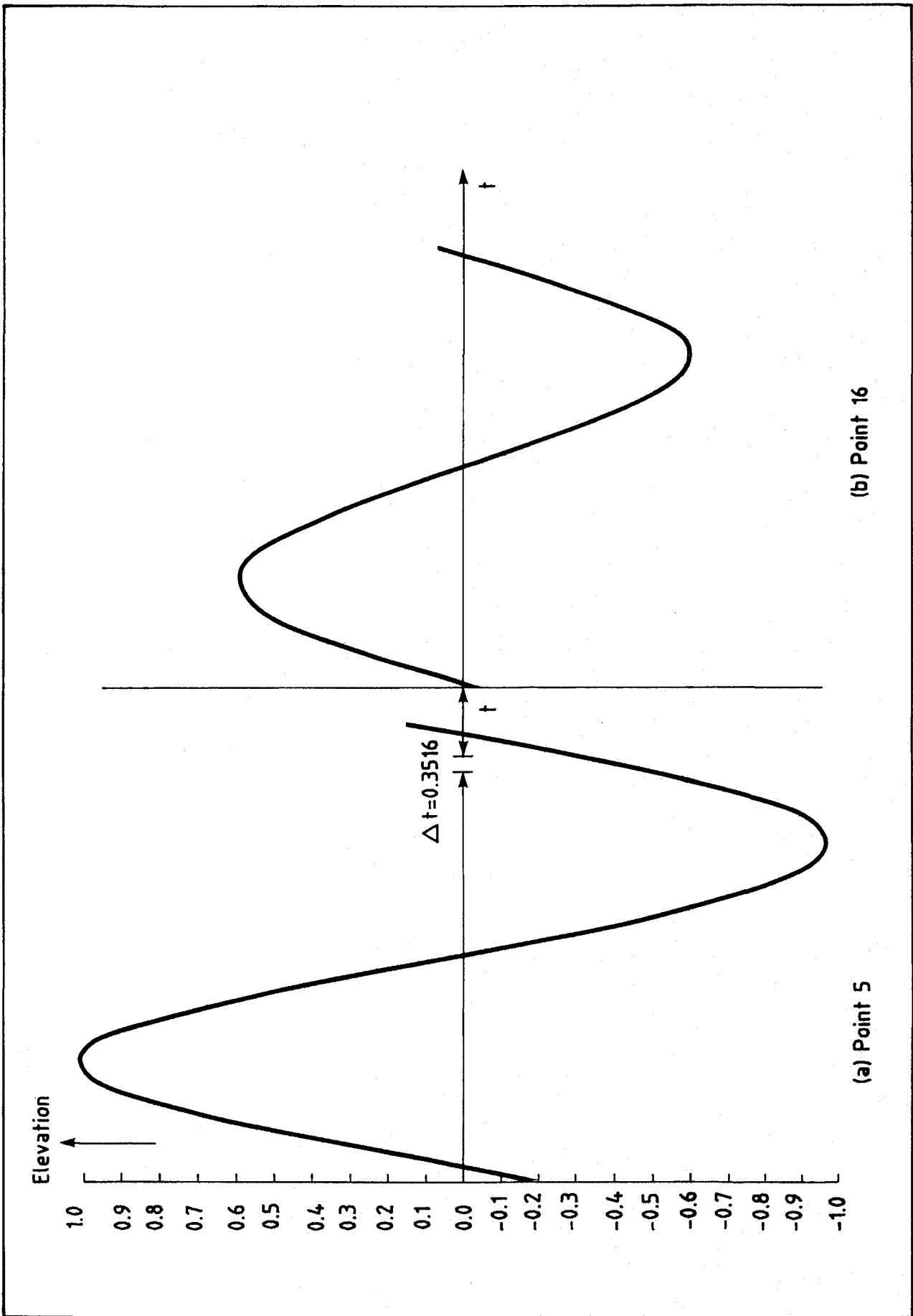


Fig 31 Wave elevation plotted against time at two surface points, period  $T=10s$ , for breakwater gap (see Fig 29) input amplitude = 1.0m

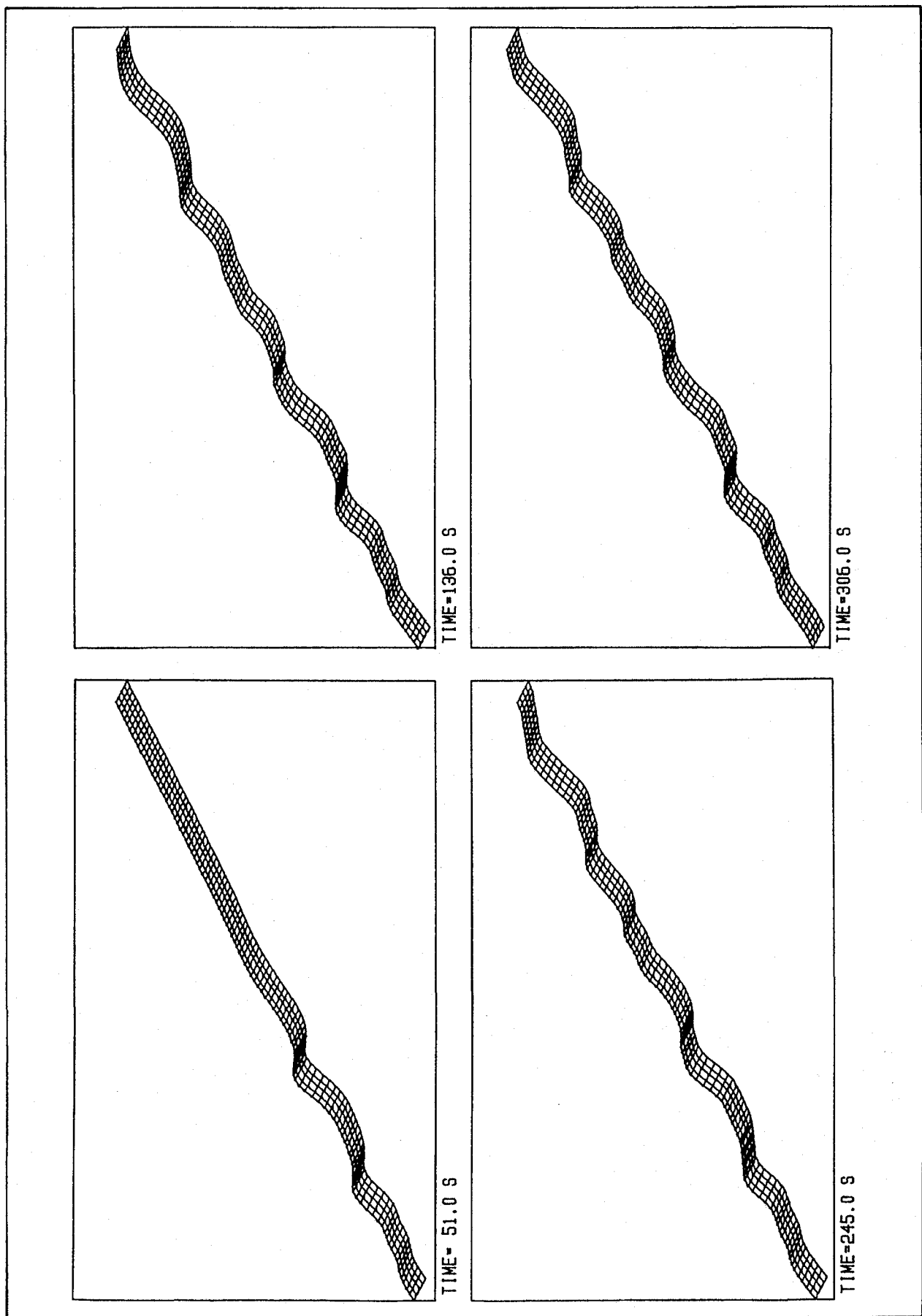


Fig 32 Surface elevations - regular wave groups

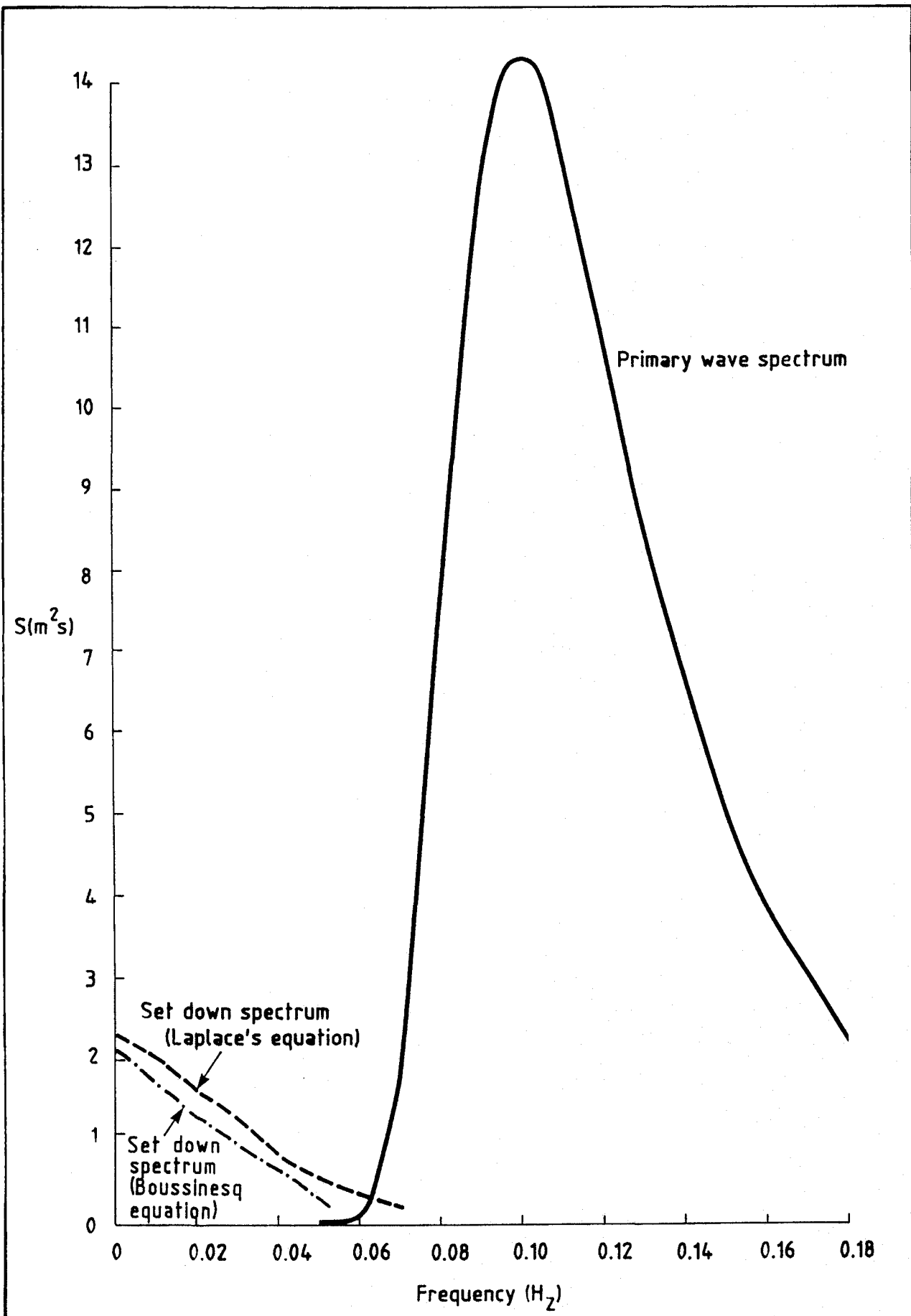


Fig 33 Spectrum for random wave input

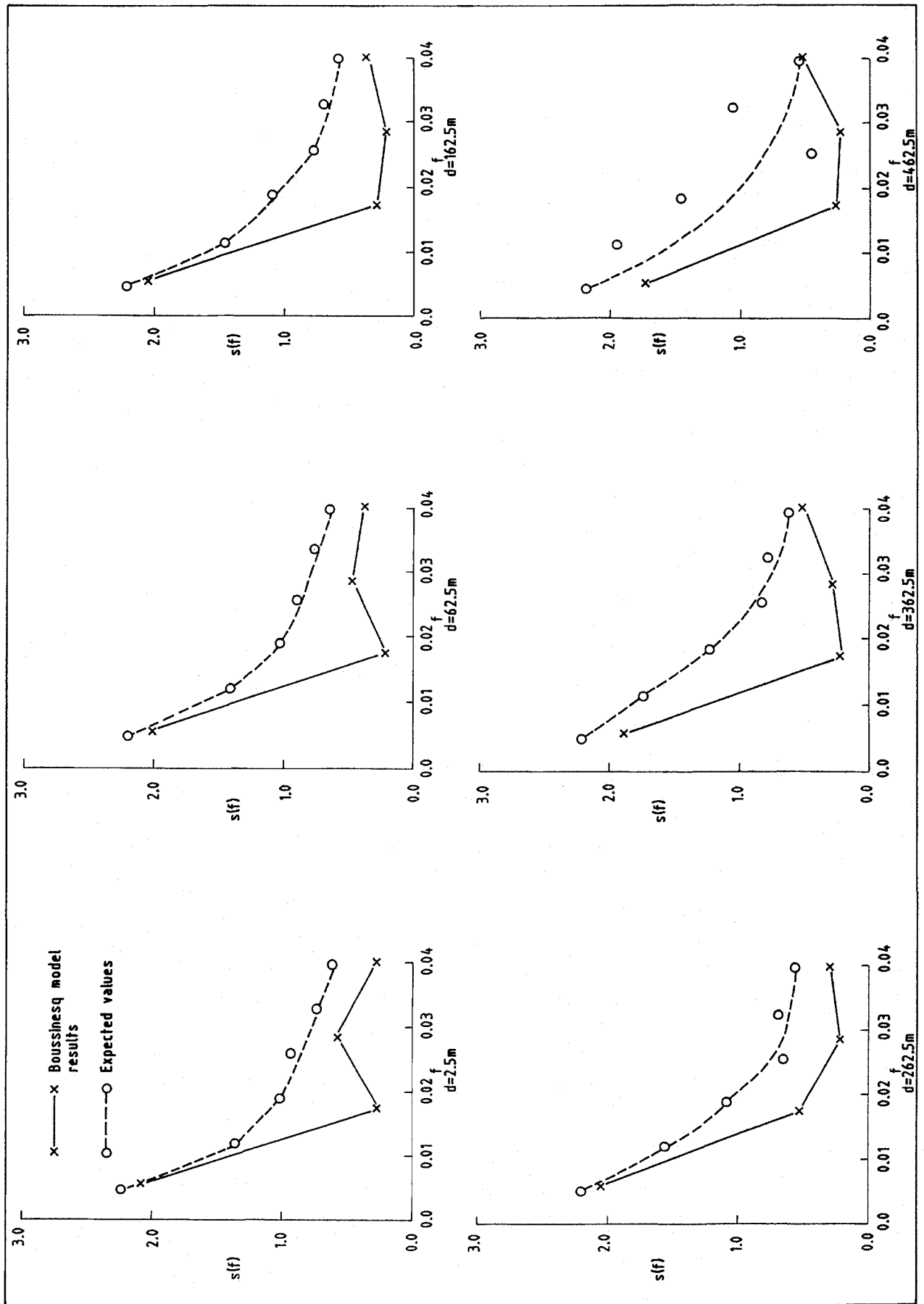


Fig 34 Spectral densities for Pierson-Moskowitz input

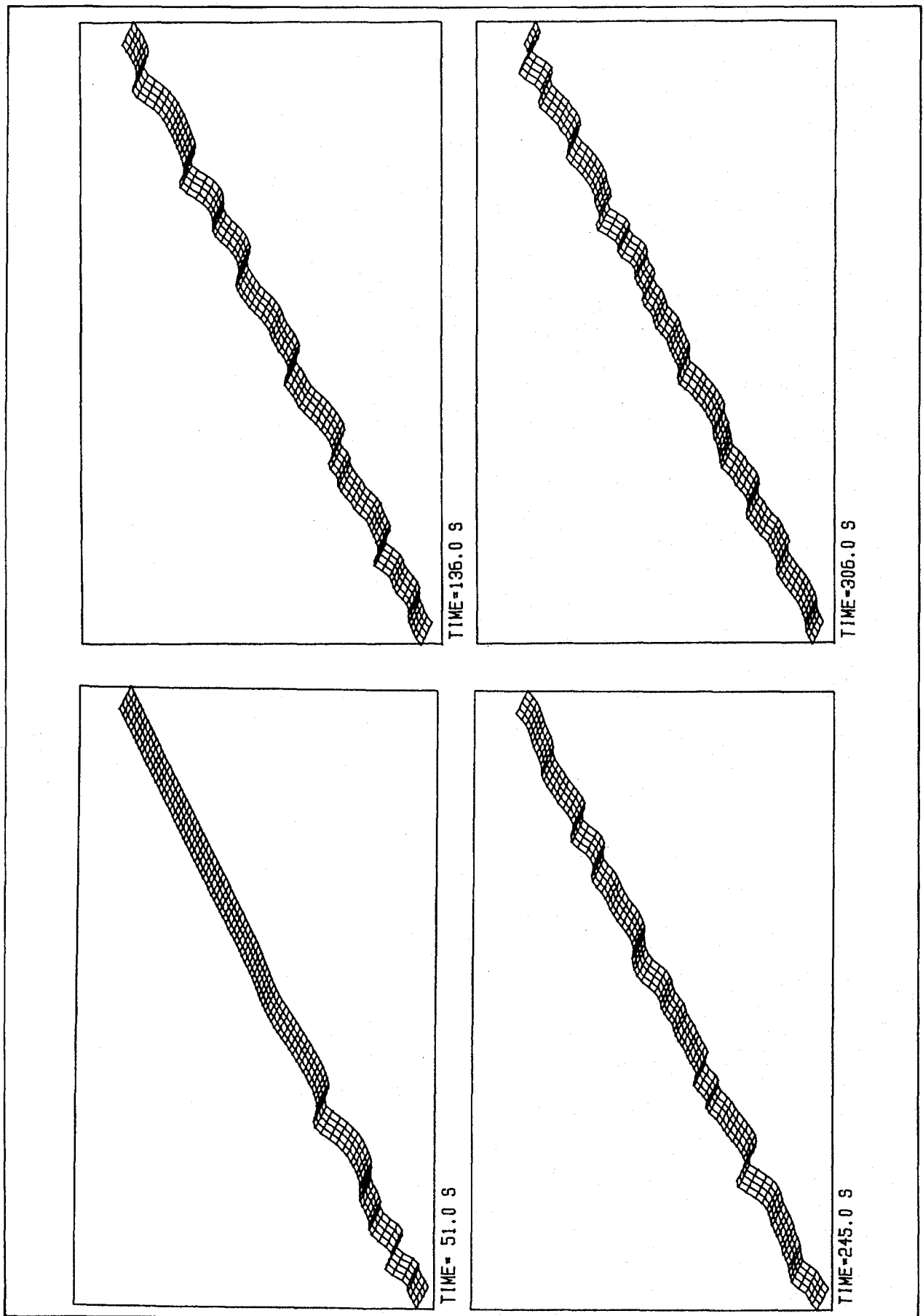


Fig 35 Surface elevations - random wave groups



**APPENDICES.**



## APPENDIX 1

### DERIVATION OF SET DOWN AMPLITUDES

**Boussinesq equation** The expression for the second order elevation for the Boussinesq equation at any point  $x$  at time  $t$  is given by

$$\eta^{(2)}(x,t) = \sum_{i=j+1}^n \sum_{j=1}^{n-1} A_{ij} \cos(\omega_{ij}t - k_{ij}x + \epsilon_{ij}), \quad (A1)$$

where  $A_{ij}$  is defined in the expressions following (3.2), and the notation of section 3.2 is retained.

By substituting  $m = i-j$ , equation (A1) can be rewritten as

$$\eta^{(2)}(x,t) = \sum_{m=1}^{n-j} \sum_{j=1}^{n-1} A_{j+mj} \cos(\omega_{j+mj}t - k_{j+mj}x + \epsilon_{j+mj}) \quad (A2)$$

It should be observed that the term  $\omega_{j+mj}$  is independent of  $j$  as,

$$\begin{aligned} \omega_{j+mj} &= \omega_{j+m} - \omega_j \\ &= 2\pi (f_{j+m} - f_j) \\ &= 2\pi \Delta f ((j+m - \frac{1}{2}) - (j - \frac{1}{2})) \\ &= 2\pi \Delta f m. \end{aligned}$$

again reference should be made to the notation of section 3.2. To make the dependence of  $\omega_{j+mj}$  clear we will write

$$\omega_m^- \equiv \omega_{j+mj} = 2\pi \Delta f m,$$

so that (A2) becomes

$$\eta^{(2)}(x,t) = \sum_{m=1}^{n-j} \sum_{j=1}^{n-1} A_{j+mj} \cos(\omega_m^- t - k_{j+mj}x + \epsilon_{j+mj})$$

The above can be rewritten as,

$$\eta^{(2)}(x,t) = \sum_{m=1}^{n-1} \sum_{j=1}^{n-k} A_{j+mj} \cos(\omega_m^- t - k_{j+mj} x + \epsilon_{j+mj}),$$

which allows us to put the expression for second order elevation in the following form:

$$\eta^{(2)}(x,t) = \sum_{m=1}^{n-1} D_m \cos(\omega_m^- t + \delta_m). \quad (A3)$$

In equation (A3)  $D_m$  is the set down amplitude associated with the difference frequency  $\omega_m^-$ , which is given by,

$$D_m^2 = \left( \sum_{j=1}^{n-m} A_{j+mj} \cos(\epsilon_{j+mj} - k_{j+mj} x) \right)^2 + \left( \sum_{j=1}^{n-m} A_{j+mj} \sin(\epsilon_{j+mj} - k_{j+mj} x) \right)^2, \quad (A4)$$

and  $\delta_m$  is such that

$$\tan \delta_m = \frac{\sum_{j=1}^{n-m} A_{j+mj} \sin(\epsilon_{j+mj} - k_{j+mj} x)}{\sum_{j=1}^{n-m} A_{j+mj} \cos(\epsilon_{j+mj} - k_{j+mj} x)} \quad (A5)$$

Laplace's equations  
and free surface  
boundary condition

Using a similar analysis to that given above for equation (3.4) it can be shown that the second order elevation term can be written in the form,

$$\eta^{(2)}(x,t) = \sum_{m=1}^{n-1} \bar{D}_m \cos(\bar{\omega}_m^- t + \bar{\delta}_m), \quad (A6)$$

where  $\bar{D}_m$  is the set down amplitude associated with the difference frequency  $\bar{\omega}_m^-$ . Following equations (A4) and (A5)  $\bar{D}_m$  and  $\bar{\delta}_m$  are given by

$$\begin{aligned} \bar{D}_m^2 &= \left( \sum_{j=1}^{n-m} \bar{A}_{j+mj} \cos(\epsilon_{j+mj} - k_{j+mj}x) \right)^2 \\ &+ \left( \sum_{j=1}^{n-m} \bar{A}_{j+mj} \cos(\epsilon_{j+mj} - k_{j+mj}x) \right)^2 \end{aligned} \quad (A7)$$

and

$$\tan \bar{\delta}_m = \frac{\sum_{j=1}^{n-m} \bar{A}_{j+mj} \sin(k_{j+mj}x - \epsilon_{j+mj})}{\sum_{j=1}^{n-m} \bar{A}_{j+mj} \cos(k_{j+mj}x - \epsilon_{j+mj})}, \quad (A8)$$

where  $\bar{A}_{ij}$ ,  $j = 1$  to  $n-1$ ,  $i = j+1$ ,  $n$  is given by the expression following equation (3.4).

Equations (A4) and (A7) can be used to calculate the set down amplitude for a particular difference frequency resulting from the Boussinesq equations, and from Laplace's equation and its free surface boundary conditions.

